De Angelis M, Giaralis A, Petrini F and Pietrosanti D. (2019) Optimal tuning and assessment of inertial dampers with grounded inerter for vibration control of seismically excited base-isolated systems. *Engineering Structures*, 196: 109250. DOI: 10.1016/j.engstruct.2019.05.091.

Optimal tuning and assessment of inertial dampers with grounded inerter for vibration control of seismically excited base-isolated systems

Maurizio De Angelis[1*], Agathoklis Giaralis[2], Francesco Petrini[3] and Daniele Pietrosanti[4]

[1,3,4] Department of Structural and Geotechnical Engineering, Sapienza University of Rome, Rome, Italy
[2] Department of Civil Engineering, City, University of London, London, UK
* Corresponding author: *maurizio.deangelis@uniroma1.it*, +39 0644585109, +39 0644585292

Summary
In this paper, the concept of an ideal grounded linear inerter, endowing supplemental inertia to passive linear tuned mass-dampers (TMDs) through its inertance property without increasing the TMD mass, is considered to reduce lateral displacement demands in base isolated structural systems (BISs). Optimal tuned mass-damper-inerter (TMDI) design parameters are numerically determined to maximize energy dissipation by the TMDI under stationary white noise support excitation. Performance of these optimally designed TMDI-equipped BISs is assessed for stationary white and colored noise excitations as well as for four recorded earthquake acceleration ground motions (GMs) with different non-stationary frequency content. It is found that for fixed mass ratio the inclusion of the grounded inerter reduces significantly secondary mass displacement and stroke for all considered excitations while it improves appreciably BIS displacement demands except for the particular case of a near-fault accelerogram characterized by early arrival of a high-energy low-frequency pulse as captured in its wavelet spectrogram. More importantly, it leads further to reductions to BIS acceleration demands with the exception of colored noise excitation for which an insignificant increase is noted. The positive effects of the inerter saturate with increasing inertance and BIS damping ratio demonstrating that small inertance values are more effective in vibration suppression of BISs with low inherent damping. Overall, it is recommended to combine low damping isolation layers with large inertance and low secondary mass TMDIs.

KEYWORDS
Inerter, Tuned Mass Damper Inerter (TMDI), Tuned Mass Damper (TMD), Tuned Inerter Damper (TID), Base isolation, Optimal design, Random excitation, Pulse-like accelerograms.

1 | INTRODUCTION

Over the past three decades, base isolation has become a widely considered passive vibration control strategy to protect bridges (e.g., [1]), buildings (e.g. [2-3]), critical structured facilities (e.g., [4-6]), and secondary sensitive components housed within structures (e.g., [7-8]) from earthquake induced horizontal ground vibration. It relies on inserting a laterally flexible (isolation) layer comprising elastomeric and/or sliding bearings in between the structure/object to be protected (superstructure) and its base/foundation. This provision results in a base-isolated system (BIS) with significantly longer fundamental natural period compared to the fixed-based (i.e., non-isolated) structure. Accordingly, the BIS attracts appreciably lower lateral seismic/inertial forces and develops reduced peak accelerations under typical seismic ground motion (GM) excitations vis-à-vis the non-isolated structure. Further, the dominant long-period vibration mode of typical BISs involves lateral rigid-body-like translation of the superstructure leading to reduced seismic deformations (e.g., inter-storey drifts in buildings). However, the above benefits come at the price of considerable lateral seismic displacement demands posed to the bearings of the isolation layer which may be detrimental to the bearings stability and to the overall structural integrity of BISs. Such demands become critical for GMs rich in low frequency content which may potentially resonate with the dominant BIS natural period (e.g., [9]), while use of supplemental viscous damping in the isolator layer to mitigate these demands increases superstructure peak response acceleration [10]. Increased acceleration response is

detrimental to secondary (sensitive) equipment housed in base-isolated buildings, to vehicles travelling on the deck of isolated bridges during seismic events, and to rocking response of base-isolated objects/artifacts.

To this end, a number of researchers [11-16] explored the potential of the tuned mass-damper (TMD), i.e., the most widely used passive linear inertial damper in vibration control applications [17], to mitigate lateral drifts in BISs. The latter strategy, involves attaching a free-to-vibrate mass to the isolation layer of the BIS via a viscoelastic link (i.e., linear spring/stiffener in parallel with a linear viscous damper) tuned/designed such that significant kinetic energy is transferred from the BISs to the attached (secondary) mass and eventually dissipated by the damper. Yang et al. [11] was the first to demonstrate the effectiveness and applicability of TMDs to reduce lateral seismic drifts in base-isolated high-rise buildings. Tsai [12] highlighted the importance of accounting for the effective damping properties of typical BISs in TMD design/tuning and further demonstrated, by examining the response of a 5-storey base isolated building to four recorded GMs, that the effectiveness of TMDs to suppress BIS displacement depends strongly on the frequency content of GMs. Similar conclusions were reached by Palazzo et al. [13] and Hoang et al. [14] by examining displacement response statistics of TMD-equipped two degree-of-freedom (DOF) and single-DOF (SDOF) models of BISs, respectively, exposed to stationary stochastic ground excitation. More importantly, Tanigushi et al. [15] concluded that the provision of a TMD reduces *both* peak BIS displacement and acceleration by considering the response of TMD-equipped SDOF BISs exposed to 12 recorded GMs. Lastly, Petti et al. [16] confirmed experimentally all previous conclusions through small-scale shaking table testing of a TMD-equipped three-DOF BIS to different recorded GMs.

Despite TMD beneficial effect for seismic response reduction in BISs, the above reviewed studies report the following drawbacks (a) excessively large secondary mass is required (i.e., of the order of 30% the mass of the superstructure or more) to achieve significant seismic drift demand reduction [11-12, 14], while the rate of reduction saturates with increasing secondary mass [12-13]; (b) secondary mass displacement can be as large as 2 to 4 times of the isolation layer displacement [15], which calls for sufficient clearance for the TMD while increases the up-front cost of the TMD dampers.

To address the above common TMD shortcomings (see also [18] and references therein) for mitigating displacement demands of BISs, this paper considers supporting the TMD secondary mass to the ground by an *ideal inerter* [19], also termed *gyro-mass damper* in the literature [20]. The ideal inerter is a linear massless two-terminal mechanical element developing a resisting force proportional to the relative acceleration of its terminals with proportionality constant, "inertance", measured in mass (kg) unit [19]. Therefore, fixing one terminal of the inerter to the ground and the other to the secondary mass of the TMD yields a linear inertial damper, termed tuned mass-damper-inerter (TMDI) by Marian and Giaralis [21], with total inertia given by the sum of the inertance and the secondary mass and with weight contributed only by the secondary mass. In this regard, it was found that the TMDI can efficiently tackle the constraints related to the size/weight of the TMD secondary mass while achieving enhanced vibration control *in non-isolated structures*. Specifically, it was demonstrated that, through optimal tuning for host/primary structure deformation reduction, the incorporation of a grounded inerter reduces significantly the required secondary mass to achieve a prescribed performance level or, equivalently, achieves significantly improved performance for the same secondary mass under stationary white noise [21] and harmonic [22] base excitation. Further, Pietrosanti et al. [23] established the potential of the TMDI optimally designed for a number of different criteria to protect lightly damped SDOF structures under earthquake excitations and reported that the grounded inerter reduces significantly secondary mass displacement demands and enhances robustness to detuning effects. Moreover, Lazar et al. [24] reported that the optimal placement of the tuned inerter-damper (TID), that is, a TMDI with no secondary mass, for efficient seismic protection of linear damped multi-storey buildings is at the ground floor in which case the inerter is grounded. More recently, Giaralis and Taflanidis [25] provided further numerical evidence of the effectiveness

of TMDI with grounded inerter to reduce inter-storey drifts, floor accelerations, and secondary mass displacement in multi-storey buildings subject to stationary colored noise ground excitation over the classical TMD.

In this respect, coupling the TMD with a grounded inerter for seismic drift demand mitigation in BISs is herein motivated by the above advantages of the TMDI over the TMD as well as by the facts that: (1) the secondary mass in TMD-equipped BISs is typically located close to the BIS support making readily feasible the incorporation of a grounded inerter, and (2) recently, a number of relatively compact and lightweight vibration control devices for earthquake engineering applications incorporating inerters with several thousands of tons of inertance have been prototyped and experimentally verified (see e.g., [26] and references therein). The above two points justify the consideration of large inertia TMDIs contributed mostly by the inertance property of the grounded inerter rather than by the secondary mass for efficient BIS vibration control.

Previous work on ground-supported inertial dampers in base-isolated structures and contributions

Table 1 provides a non-exhaustive list of previous studies considering ground-supported inertial dampers with various element/device configurations for vibration control of support-excited BISs codified in Figure 1 for compactness in exposition. Optimal inertial damper design and/or assessment criteria used in gauging the inertial dampers effectiveness for the purpose at hand are also reported in Table 1, while the last entry of the table pertains to this work for the sake of comparison and for highlighting contributions.

Historically, Zhang and Iwan [27] were the first to consider a ground-supported inertial damper for vibration suppression of base isolated buildings. It comprised a TMD attached to the ground with secondary mass connected through a semi-actively controlled Coulomb friction (fuse) element to the BIS. Through parametric analysis, optimal tuning of the damper parameters against 8 recorded near-fault GMs was achieved and isolation layer drift reduction was reported at the expense of external power requirements to operate the fuse element leveraging the control force applied to the BIS. Further, Saito et al. [28] considered a non-optimally tuned viscous mass damper (VMD) comprising a dashpot in parallel with an inerter element supported to the ground via a linear spring, to mitigate the response of base-isolated building structures. Some practical recommdendations were made as to the inertance required to suppress BIS response in view of limited results for a single artificial GM assuming no damping in the isolation layer. More recently, Zhao et al. [26] considered the potential of an optimally tuned to white noise excitation VMD rigidly supported to the ground and viscoelastically connected to a BIS with no damping in the isolation layer. Response history analysis results for 5 recorded and 4 artificial GMs showed that the adopted configuration and optimal tuning strategy is sufficient to reduce BIS displacement and acceleration concurrently. Saitoh [20] explored the potential of a grounded inerter connected directly to a BIS to reduce BIS seismic demands vis-à-vis two other configurations involving non-grounded inerters (see Table 1). Based on response history analysis for three GMs to systems optimally designed for harmonic excitation, it was concluded that a grounded inerter alone was ineffective in suppressing high frequency dynamics and therefore detrimental to BIS acceleration. Moreover, Xiang et al. [29] considered non-conventional TMDs with grounded dashpot optimally designed for peak BIS drift minimization under harmonic excitation and noted improved performance compared to classical TMDs as well as reduced secondary mass displacement based on response history results for three different GMs. Lately, De Domenico and Ricciardi [30] put forth a hybrid base isolation system tailored for building structures comprising a low-damping set of grounded isolators and a high-damping set of isolators connected to the ground through inerters and demonstrated its superiority compared to conventional base isolation for colored noise excitation as well as for a number of recorded GMs.

De Angelis M, Giaralis A, Petrini F and Pietrosanti D. (2019) Optimal tuning and assessment of inertial dampers with grounded inerter for vibration control of seismically excited base-isolated systems. *Engineering Structures*, 196: 109250. DOI: 10.1016/j.engstruct.2019.05.091.

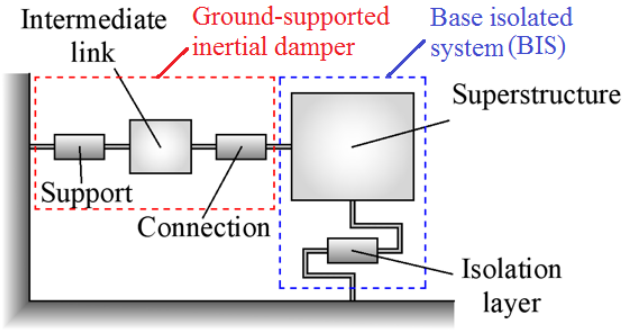

FIGURE 1 Block representation of generic ground-supported inertial dampers in base-isolated structures (to be studied together with Table 1)

TABLE 1 Ground-supported inertial dampers in base-isolated structures (to be studied together with Fig.1)

Reference	**Elements/models used in different blocks of Figure 1**					**Optimal tuning and/or parametric performance assessment**
	Support	Intermediate link	Connection	Superstructure	Isolation layer	
Zhang and Iwan [27]	VE	Mass	CF	5-storey shear frame	VE	parametric analysis for BIS response minimization to 8 near-fault GMs
Saito et al. [28]	Elastic	VMD	Rigid	7-storey shear frame	Elastic	parametric analysis for one artificial GM
Saitoh [20]	Rigid	Inerter	Rigid	Rigid block	VE	minimization of BIS response to harmonic excitation and sensitivity analysis for 3 recorded GMs
	VE	Inerter				
	VE	VMD				
Xiang et al. [29]	Dashpot	Mass	Elastic	SDOF oscillator	VE	minimization of BIS response to harmonic excitation and sensitivity analysis for 3 recorded GMs
Zhao et al. [26]	Rigid	VMD	VE	SDOF oscillator	Elastic	minimization of BIS response to white noise excitation and sensitivity analysis for 9 GMs
De Domenico and Ricciardi [30]	Inerter	-	VE	1-storey building	VE	optimization against 3 different criteria for white noise excitation and assessment for 8 GMs
				5-storey building frame		Energy-based optimization for colored noise and assessment for stationary artificial GMs
This paper	Inerter	Mass	VE	Rigid block	VE	Energy-based optimization for white noise and assessment for two different colored noise and 4 GMs
	Inerter	-	VE			
	-	Mass	VE			

VE: visco-elastic (linear spring in parallel with dashpot)
CF: Coulomb friction element (damper)
VMD: viscous mass damper (linear inerter in parallel with dashpot)

Notably, most of previous works on ground-supported inertial dampers aimed for enhanced seismic input energy dissipation in BISs by using an inerter in parallel to a dashpot (i.e., the VMD in Table 1) to amplify the relative motion of the viscous damper terminals. Quite differently, in the TMDI configuration the (grounded) inerter amplifies the effective inertial property of a conventional TMD for improved BIS vibration suppression as achieved by large-mass TMDs. In fact, in terms of dynamical modelling, the herein studied TMDI bears close resemblance only to the hybrid isolation system of De Domenico and Ricciardi [30]. Further, both works employ the same energy-based optimal design criterion, firstly considered by Pietrosanti et al. [23] for TMDI tuning. Nevertheless, the aims and objectives of the present work are different from De Domenico and Ricciardi [30] as, rather than proposing a new base-isolation system applicable to buildings, the focus here is on conceptualizing the use of the grounded inerter to TMD-equipped BISs and on quantifying beneficial

effects of large inertia TMDIs through large inertance vis-à-vis large secondary mass for different effective isolation layer damping levels accounting for the frequency content of the support excitation. In this regard, novel contributions of this work include: (I) quantification of BIS and of secondary mass kinematics on the TMDI inertance-secondary mass plane and performance interpretation based on complex modal analysis results for energy-based optimally tuned TMDI-equipped BISs; (II) assessment of vibration suppression effectiveness achieved through energy dissipation by the inertial damper vis-à-vis energy dissipation by the isolation layer for white and for colored noise support excitation; and (III) appraisal of response history analysis results from optimally tuned TMDI-equipped BISs subject to recorded GMs with different time-varying frequency content relying on wavelet-based GM energy maps on the natural period-time plane.

2 | GENERIC BASE-ISOLATED STRUCTURAL SYSTEM EQUIPPED WITH GROUNDED-INERTER MASS-DAMPER

2.1 | System model description, equations of motion and complex modal properties

Consider a planar BIS exposed to horizontal support acceleration $\ddot{u}_G$. The superstructure is taken as rigid and is represented by a lumped mass, m_I, resting on a flexible isolation layer as depicted in Figure 2. The oscillating mass of the isolation system is included within m_I. This is a commonly used in the literature generic model for BIS (see e.g., [31-33]) which renders subsequent numerical results and discussion relevant to different types of structures including stiff low-rise base isolated buildings (e.g., [15]), decks of isolated bridges along their longitudinal direction (e.g. [14]), base isolated storage tanks (e.g., [4-5]), and block-type secondary equipment and artifacts anchored on floor isolation systems within buildings (e.g., [7-8]). Moreover, the isolation layer is represented by linear stiffness and damping coefficients k_I and c_I, respectively, commonly used to model the behavior of different types of bearings in practical seismic design and assessment of BISs (see e.g., [34-35] and references therein).

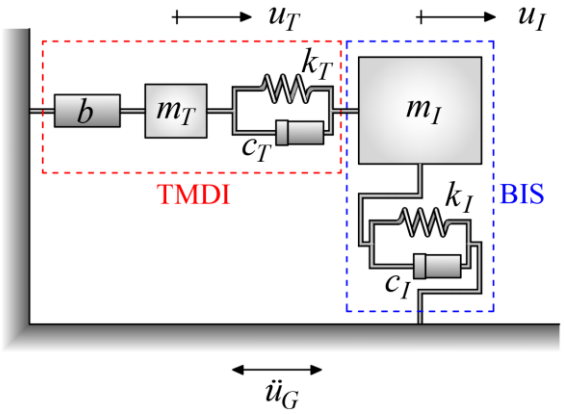

FIGURE 2 Considered 2-DOF dynamical system: BIS (primary structure)+TMDI (inertial damper)

A linear passive TMD with physical mass m_T and with stiffness and damping properties k_T and c_T, respectively, is attached to the adopted BIS model to suppress the lateral deformation of the isolation layer expressed by the relative to the ground displacement u_I of the mass m_I in Figure 2. The TMD is supported to the ground by an ideal linear inerter [19] developing a resisting force equal to $b\ddot{u}_T$, where b is the inertance device property, u_T is the relative to the ground displacement of the secondary mass m_T and, henceforth, a dot over a symbol signifies differentiation with respect to time t. To this end, a two degree of freedom (2-DOF) dynamical system is defined representing a generic BIS equipped with a grounded-inerter tuned mass damper (TMDI).

Let $\omega_I = \sqrt{k_I/m_I}$ and $\omega_T = \sqrt{k_T/(m_T + b)}$ be the uncoupled natural frequency of the BIS and of the TMDI, respectively. The governing equations of motion of the 2-DOF system in Figure 2 are written as

$$\ddot{q}_I + 2\xi_I\dot{q}_I + q_I - 2\mu_E\xi_T\nu(\dot{q}_T - \dot{q}_I) - \mu_E\,\nu^2(q_T - q_I) = -\ddot{q}_G \quad (1)$$

$$\mu_E\ddot{q}_T + 2\mu_E\xi_T\nu(\dot{q}_T - \dot{q}_I) + \mu_E\nu^2(q_T - q_I) = -\mu\ddot{q}_G \quad (2)$$

in terms of the non-dimensional relative to the ground displacement coordinates $q_I = u_I/(g/\omega_I^2)$ and $q_T = u_T/(g/\omega_I^2)$ and normalized excitation $\ddot{q}_G = \ddot{u}_G/g$, where g is the acceleration of gravity. In the above equations, the non-dimensional damping ratio of the BIS, ξ_I, damping ratio of the TMDI, ξ_T, uncoupled frequencies ratio, ν, mass ratio, μ, inertance ratio, β, and effective TMDI inertial ratio, μ_E, are defined as

$$\xi_I = \frac{c_I}{2m_I\omega_I}\ ;\ \xi_T = \frac{c_T}{2(m_T + b)\omega_T}\ ;\ \nu = \frac{\omega_T}{\omega_I}\ ;\ \mu = \frac{m_T}{m_I}\ ;\ \beta = \frac{b}{m_I}\ ;\ \mu_E = \mu + \beta \quad (3)$$

Notably, by setting $(b =)\beta = 0$ (i.e. $\mu_E = \mu$), the considered 2-DOF system in Figure 2 coincides with the model considered in [15] for a BIS equipped with a classical TMD hereafter denoted by BIS+TMD. Further, by setting $(m_T =)\mu = 0$ (i.e. $\mu_E = \beta$), the 2-DOF system in Figure 2 degenerates to a BIS equipped with the tuned inerter damper (TID) in [24] hereafter denoted by BIS+TID in which case q_T traces the displacement of the non-grounded inerter terminal. In the numerical part of this work, the limiting cases of $(b =)\beta = 0$ (no inerter) and of $(m_T =)\mu = 0$ (no secondary mass) are studied as special cases of the BIS+TMDI system of Figure 2 to draw useful comparisons on the efficacy of TMD, TID, and TMDI for vibration control of BISs.

2.2 | State-space formulation and complex modal analysis

The Eqs. (1-2) of the dynamical system in Figure 2 are cast in state space as

$$\begin{aligned}\dot{\mathbf{z}}(t) &= \mathbf{A}_s\mathbf{z}(t) + \mathbf{B}_s\ddot{q}_G(t)\\ \boldsymbol{\theta}(t) &= \mathbf{C}_s\mathbf{z}(t)\end{aligned} \quad (4)$$

where

$$\mathbf{A}_s = \begin{bmatrix} 0 & 0 & 1 & 0 \\ 0 & 0 & 0 & 1 \\ -\mu_E\nu^2 - 1 & \mu_E\nu^2 & -2(\xi_I + \mu_E\nu\xi_T) & 2\mu_E\nu\xi_T \\ \nu^2 & -\nu^2 & 2\nu\xi_T & -2\nu\xi_T \end{bmatrix};\ \mathbf{B}_s = \begin{bmatrix} 0 \\ 0 \\ -1 \\ -\mu/\mu_E \end{bmatrix};\ \mathbf{C}_s = \begin{bmatrix} 1 & 0 & 0 & 0 \\ 0 & 1 & 0 & 0 \\ 0 & 0 & 1 & 0 \\ -1 & 1 & 0 & 0 \\ 0 & 0 & 1 & -1 \end{bmatrix} \quad (5)$$

In Eq.(4), $\mathbf{z}(t) = (q_I \quad q_T \quad \dot{q}_I \quad \dot{q}_T)^T$ is the state vector and the superscript "T" denotes matrix transposition. Further, $\boldsymbol{\theta}(t) = (q_I \quad q_T \quad \dot{q}_I \quad q_{TI} \quad \dot{q}_{TI})^T$, where $q_{TI} = q_T - q_I$, is the vector collecting ouput variables associated with the structural performance indices defined in a subsequent sub-section.

The considered dynamical system is non-classically damped. Therefore complex modal analysis (see e.g., [36]) is employed to derive modal properties which facilitate shedding light on structural performance in the numerical part of this work. Specifically, the characteristic equation of the underlying eigenvalue problem reads as

$$s^4 + 2\big(\xi_I + \nu\xi_T(1 + \mu_E)\big)s^3 + (1 + \nu^2(1 + \mu_E) + 4\nu\xi_I\xi_T)s^2 + 2\nu(\nu\xi_I + \xi_T)s + \nu^2 = 0 \quad (6)$$

The roots of Eq. (6) are in complex conjugate pairs $s_i = \alpha_i + j\omega_i$ and $\bar{s}_i = \alpha_i - j\omega_i$; i=1,2 and the i-th mode pseudo-frequency and pseudo-damping factors are given as $\Omega_i = \sqrt{s_i\bar{s}_i}$ and $\eta_i = -Re(s_i)/\sqrt{s_i\,\bar{s}_i}$.

2.3 | System response to white and colored stochastic ground excitation

Consider first the case of the normalized support excitation $\ddot{q}_G$ being a stationary zero mean Gaussian white noise stochastic process. This case is of interest as optimally TMDI *design* is pursued in the next section for white noise support excitation following pertinent recommendations for optimal TMD design of BISs [14]. For zero initial conditions, the Gaussian response process vector $\mathbf{z}(t)$ is described by the covariance matrix $\mathbf{G_{zz}} = E[\mathbf{z}(t)\mathbf{z}(t)^T]$, where the symbol $E[\cdot]$ is the expected value operator. Focusing on steady-state stationary response, the covariance matrix satisfies the Lyapunov equation [37]

$$\mathbf{A}_s\mathbf{G_{zz}} + \mathbf{G_{zz}}\mathbf{A}_s^T + 2\pi\mathbf{B}_s\mathbf{B}_s^T = \mathbf{0}, \tag{7}$$

for unit spectral intensity white noise excitation. Equation (7) can be readily solved numerically for $\mathbf{G_{zz}}$ and the variance $\sigma_{\theta j}^2$ of the *j*-th output variable contained in vector $\boldsymbol{\theta}(t)$ is obtained by

$$\sigma_{\theta j}^2 = \mathbf{n}_j\mathbf{C}_s\mathbf{G_{zz}}\mathbf{C}_s^T\mathbf{n}_j^T \tag{8}$$

where $\mathbf{n}_j$ is a 1-by-5 vector of zeros except for its *j*-th element being equal to one.

Modelling earthquake-induced excitation by white noise is not appropriate for structural seismic performance *assessment* as it does not capture the anticipated non-white excitation frequency content for BISs either founded on the ground or housed within seismically excited structures. Therefore, the case of $\ddot{q}_G$ being a stationary zero mean Gaussian colored noise stochastic process is considered to *assess* structural performance of BIS+TMDI systems represented in the domain of circular frequency ω by the filtered Kanai-Tajimi spectrum [38]

$$S_g(\omega) = \frac{\omega_g^4 + 4\zeta_g^2\omega^2\omega_g^2}{\left(\omega_g^2 - \omega^2\right)^2 + 4\zeta_g^2\omega_g^2\omega^2}\frac{\omega^4}{\left(\omega_f^2 - \omega^2\right)^2 + 4\zeta_f^2\omega_f^2\omega^2}\,. \tag{9}$$

In the above equation the Kanai-Tajimi parameters ω_g and ζ_g represent the resonance frequency and damping properties, respectively, of the BIS supporting ground, or host structure, modeled as a linear damped SDOF oscillator driven by white noise. Further, the parameters ω_f and ζ_f control the cut-off frequency and the "steepness" of a high-pass filter used to suppress spurious low frequency content which may influence the response of flexible BISs. The excitation model in Eq.(9) is written in state space form as

$$\begin{aligned}\dot{\mathbf{x}}(t) &= \mathbf{A}_g\mathbf{x}(t) + \mathbf{B}_g w(t)\\ \ddot{q}_G(t) &= \mathbf{C}_g\mathbf{x}(t)\end{aligned} \tag{10}$$

where $\mathbf{x}(t) = (x_g \quad x_f \quad \dot{x}_g \quad \dot{x}_f)^T$ is the state vector of the excitation model with x_g being the response/output of the first (Kanai-Tajimi) filter and x_f being the response/output of the second (high-pass) filter, $w(t)$ is a unit variance Gaussian zero mean white noise process, and

$$\mathbf{A}_g = \begin{bmatrix} 0 & 1 & 0 & 0 \\ -\omega_g^2 & -2\zeta_g\omega_g & 0 & 0 \\ 0 & 0 & 0 & 1 \\ -\omega_g^2 & -2\zeta_g\omega_g & -\omega_f^2 & -2\zeta_f\omega_f \end{bmatrix} \;;\quad \mathbf{B}_g = \begin{bmatrix} 0 \\ 1 \\ 0 \\ 0 \end{bmatrix} \;;\quad \mathbf{C}_g = \frac{S_o}{g^2}\begin{bmatrix} -\omega_g^2 \\ -2\zeta_g\omega_g \\ \omega_f^2 \\ 2\zeta_f\omega_f \end{bmatrix}^T \tag{11}$$

The state space representations in Eqs. (4) and (10) can be readily combined in the single state space model (see e.g., [39])

$$\begin{aligned}\dot{\mathbf{y}}(t) &= \mathbf{A}\mathbf{y}(t) + \mathbf{B}w(t)\\ \boldsymbol{\varphi}(t) &= \mathbf{C}\mathbf{y}(t)\end{aligned} \tag{12}$$

where $\mathbf{y}(t) = (\mathbf{z}^T(t) \quad \mathbf{x}^T(t))$ is the state vector of the combined BIS+TMDI 2-DOF system with the ground excitation model in Eq.(9), $\boldsymbol{\varphi}(t) = \boldsymbol{\theta}(t)$ is the output vector and

$$\mathbf{A} = \begin{bmatrix} \mathbf{A}_{\mathrm{S}} & \mathbf{B}_{\mathrm{S}}\mathbf{C}_{\mathrm{g}} \\ \mathbf{0}_{4\mathrm{x}4} & \mathbf{A}_{\mathrm{g}} \end{bmatrix} \quad ; \quad \mathbf{B} = \begin{bmatrix} \mathbf{0}_{4\mathrm{x}1} \\ \mathbf{B}_{\mathrm{g}} \end{bmatrix} \quad ; \quad \mathbf{C} = [\mathbf{C}_{\mathrm{S}} \quad \mathbf{0}_{5\mathrm{x}4}] \tag{13}$$

The combined model in Eq.(12) is white-noise excited and therefore, its covariance matrix, $\mathbf{G_{yy}} = E[\mathbf{y}(t)\mathbf{y}(t)^T]$, satisfies a Lyapunov equation similar to Eq. (7) which can be numerically solved for $\mathbf{G_{yy}}$ [39]

$$\mathbf{A}\mathbf{G_{yy}} + \mathbf{G_{yy}}\mathbf{A}^T + 2\pi\mathbf{B}\mathbf{B}^T = \mathbf{0}. \tag{14}$$

The variance $\sigma^2_{\varphi j}$ of the *j*-th output variable of interest contained is obtained as

$$\sigma^2_{\varphi j} = \mathbf{m}_j\mathbf{C}\mathbf{G_{yy}}\mathbf{C}^T\mathbf{m}_j^T \tag{15}$$

in a similar manner as in the case of a white-noise excited BIS+TMDI system, where $\mathbf{m}_j$ is a 1-by-9 vector of zeros except for its *j*-th element being equal to one.

2.4 | Adopted structural performance indices for stochastic seismic excitation

For both white noise and colored noise stochastic excitations, the performance of the structural system in Figure 2 is assessed in subsequent sections by using the following non-dimensional kinematic-based performance indices

$$d_I = \frac{\sigma^2_{q_I}}{\sigma^2_{q_R}} \quad ; \quad a_I = \frac{\sigma^2_{\ddot{q}_{\mathrm{I}}^{tot}}}{\sigma^2_{\ddot{q}_{\mathrm{R}}^{tot}}} \quad ; \quad d_T = \frac{\sigma^2_{q_{\mathrm{T}}}}{\sigma^2_{q_{\mathrm{R}}}} \quad ; \quad d_{TI} = \frac{\sigma^2_{q_{\mathrm{TI}}}}{\sigma^2_{q_{\mathrm{R}}}} \tag{16}$$

where $\sigma^2_{\ddot{q}_{\mathrm{I}}^{tot}}$ is the variance of the total acceleration of the BIS computed upon manipulating Eq.(1) as

$$\sigma^2_{\ddot{q}_{\mathrm{I}}^{tot}} = -(1+\mu_E\,\nu^2)^2\sigma^2_{q_I} + \mu_E^2\,\nu^4\sigma^2_{q_{\mathrm{T}}} - 4(\mu_E\xi_T\nu + \xi_I)^2\sigma^2_{\dot{q}_I} + 4\mu_E^2\,\nu^2\xi_T^2\sigma^2_{\dot{q}_T} \tag{17}$$

and $\sigma^2_{q_{\mathrm{R}}}$ and $\sigma^2_{\ddot{q}_{\mathrm{R}}^{tot}}$, are the displacement and total acceleration variances of an uncontrolled reference BIS with $\xi_I = 0.15$. Furthermore, the following energy-based unitless performance index [23]

$$EDI = \frac{ED_T}{ED_I + ED_T} \leq 1 \tag{18}$$

is also considered where ED_I and ED_T are the expected values of the energy dissipated by the viscous elements of the BIS and of the TMDI, respectively, in a lapse of time Δt given as

$$ED_{\mathrm{I}} = 2\xi_I\,\sigma^2_{\dot{q}_I}\,\Delta t \quad ; \quad ED_{\mathrm{T}} = 2\mu_E\xi_T\nu\,\sigma^2_{\dot{q}_{\mathrm{TI}}}\,\Delta t \tag{19}$$

Performance indices in Eqs. (14) and (16) are computed using Eq. (8). Importantly, they are independent of the excitation intensity of the input excitation; they only depend on the frequency content of the excitation. Further, kinematic indices in Eq.(14) measure the relative performance of the BIS+TMDI in Figure 2 with respect to a reference BIS with medium-to-large seismic energy dissipation capacity, expressed through the $\xi_I = 0.15$, under the same excitation. To this end, indices d_I and a_I gauge potential performance improvement in the root-mean-square (RMS) sense to the critical peak BIS displacement relative to the ground and total acceleration seismic demands, respectively, achieved by the inclusion of the TMDI as well as by adopting $\xi_I \neq 0.15$. Moreover, indices d_T and d_{TI} monitor the secondary mass RMS displacement and stroke (i.e., secondary mass displacement relative to the BIS displacement), respectively, normalized by the RMS displacement of the uncontrolled reference BIS. The last two quantities are associated with the cost of different

TMDIs as the former is proportional to the required clearance to accommodate the secondary mass without collisions while the latter is proportional to the required extensibility of the TMDI damping and inerter devices. Lastly, the energy-based EDI index in Eq.(16) depends on all BIS+TMDI properties in Eq.(3) but is not related to any particular reference BIS. Rather, it quantifies the portion of the total seismic energy absorbed in the BIS+TMDI (i.e., $ED = ED_I + ED_T$) being dissipated by the TMDI.

3 | OPTIMAL TMDI DESIGN AND PERFORMANCE ASSESSMENT FOR WHITE NOISE EXCITED BISs

3.1 | EDI-based optimal TMDI design for BISs

To support meaningful comparisons and discussion on seismic performance improvement of BIS+TMDIs with different properties subject to seismic excitations of different frequency content, it is deemed essential to optimally design/tune the TMDI *given* a BIS exposed to *neutral*, in terms of frequency content, seismic excitation. To this aim, an optimal TMDI design problem is herein formulated aiming to maximize the EDI index in Eq.(16) for pre-specified BISs natural period, $T_I = 2\pi/\omega_I = 2\pi\sqrt{m_I/k_I}$, and damping ratio, ξ_I, exposed to white noise ground excitation.

The considered optimal design problem involves four independent design parameters namely the TMDI frequency and damping ratios grouped in the vector $\mathbf{u}_1=[\nu\ \xi_T]^T$, and the mass and inertance ratios grouped in the vector $\mathbf{u}_2=[\mu\ \beta]^T$. The optimization problem is solved numerically using standard pattern search algorithm in MATLAB® to determine optimal design parameters in $\mathbf{u}_1$ bounded within a pre-specified search range $[\mathbf{u}_1^{min}, \mathbf{u}_1^{max}]$ for different *given* values of the parameters in $\mathbf{u}_2$. This is mathematically written as

$$\max_{\mathbf{u}_1}\{EDI(\mathbf{u}_1|\mathbf{u}_2)\} \quad \text{subjected to} \quad \mathbf{u}_1^{min} \le \mathbf{u}_1 \le \mathbf{u}_1^{max} \qquad (20)(18)$$

In all the ensuing numerical work, the bounds of the search range used in solving Eq.(18) is greedily taken as $\mathbf{u}_1^{min} = [0.01\ \ 0.01]^T$ and $\mathbf{u}_1^{max} = [10\ \ 10]^T$ to exhaust any possibility that the optimal design point lies outside the search range.

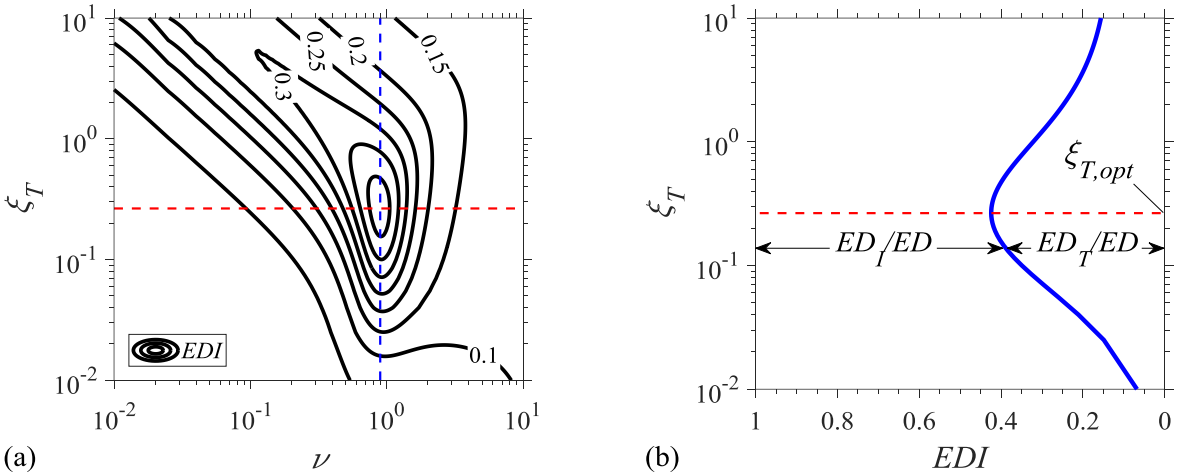

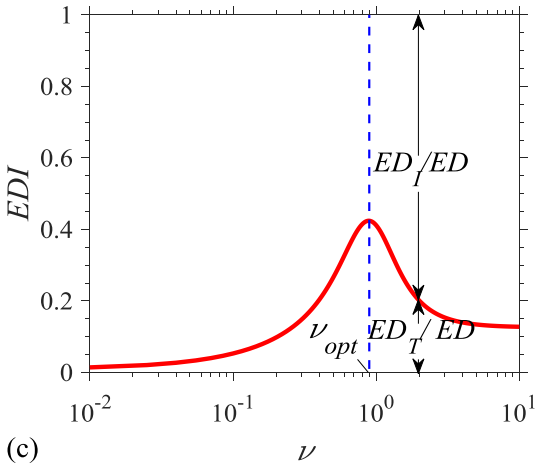

FIGURE 3 Illustration of convexity in EDI-optimal BIS+TMDI design for $\xi_I = 0.15$, $\mu = 0.05$ and $\beta = 0.20$: (a) EDI response surface contour plot; (b) EDI cross-section at optimal ξ_T and (c) EDI cross-section at optimal ν.

From a computational viewpoint, strong convex behavior of EDI on the ν-ξ_T plane is noted with a single global optimal design point being observed for all BIS+TMDI optimization cases considered. In this regard, a gradient-based optimization algorithm may well be used in solving Eq.(18) for computational efficiency. For illustration of typical convexity level observed and robustness to design parameters, Figure 3(a) presents contour plots of the EDI response surface on the ν-ξ_T design parameters plane for an arbitrarily selected BIS+TMDI and Figures 3(b) and 3(c) plot cross-sections of the EDI response surface along the broken lines of Figure 3(a) corresponding to the optimal TMDI damping ratio and TMDI frequency ratio values, respectively.

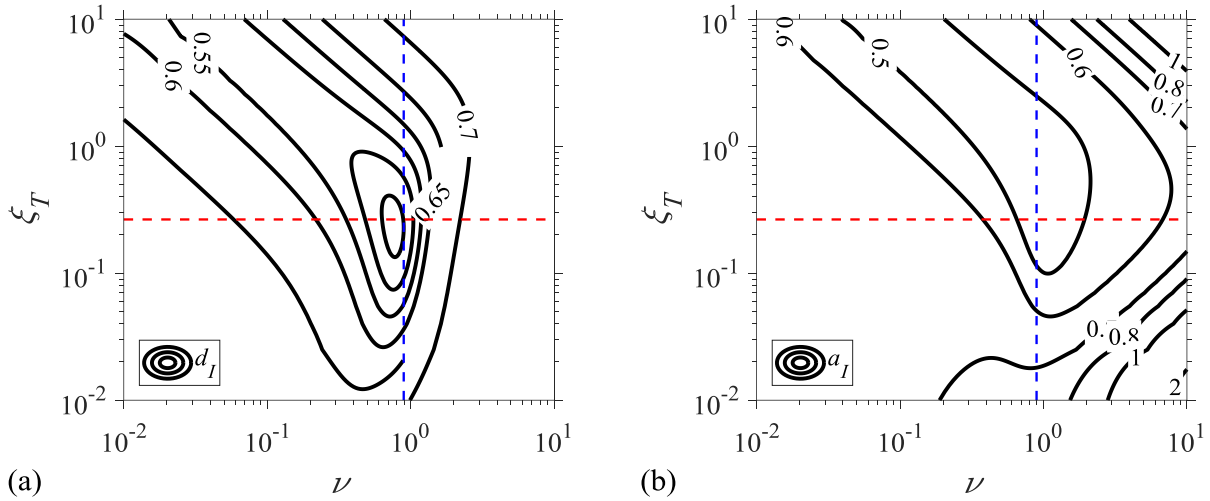

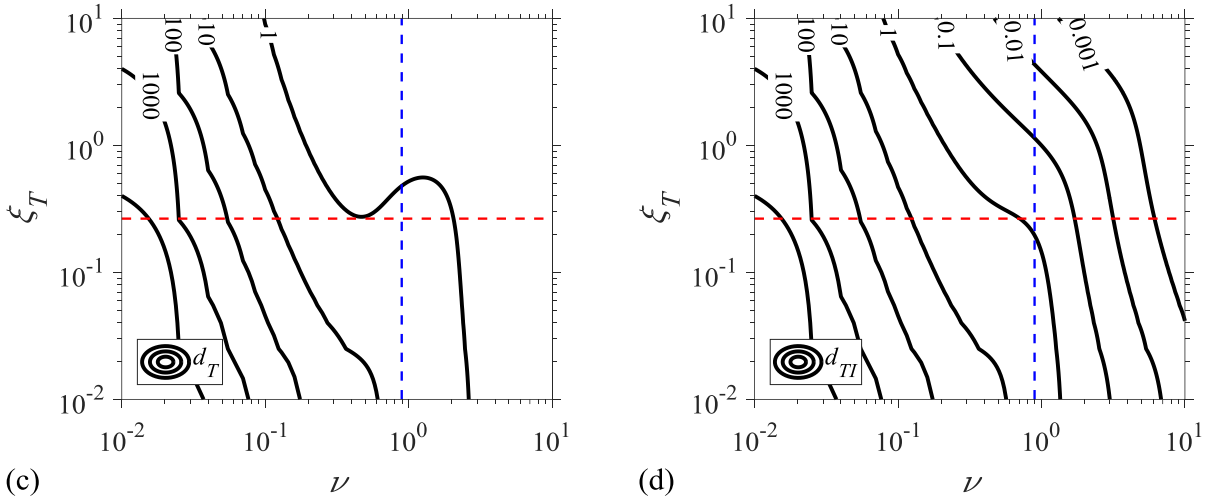

FIGURE 4 Contour plots of BIS+TMDI performance indices in Eq.(14) on the ν-ξ_T plane for $\xi_I = 0.15$, $\mu = 0.05$ and $\beta = 0.20$.

From a structural dynamics viewpoint, EDI-based optimization maximizes the portion of the energy dissipated by the TMDI, ED_T, from the total energy absorbed in white-noise excited BIS+TMDIs $ED = ED_I + ED_T$, in a given time window. For example, the peak EDI value achieved upon optimal tuning of the TMDI in Figure 3 suggests that 42% of the total absorbed energy by the entire system is dissipated by the TMDI, ED_T, with the remaining 58% being dissipated at the isolation layer, ED_I. For any non-optimal (ν, ξ_T) pair of design parameters, less than 42% of the total energy absorbed is dissipated by the TMDI as indicated in Figures 3(b) and 3(c). Further insight on BIS+TMDI performance achieved by EDI-based optimal TMDI tuning is gained by examining the contour plots of performance indices in Eq. (14) on the ν-ξ_T plane furnished in Figure 4 in which the location of the optimal design parameters is indicated by broken lines. It is seen that neither the normalized displacement d_I nor the acceleration a_I are minimized, though the EDI-optimal ν_{opt} and $\xi_{T,opt}$ parameters do lie *concurrently* close to those that would minimize d_I and to those that would minimize a_I. Therefore, EDI-based optimization does serve well the purpose of efficient simultaneous RMS BISs displacement and absolute acceleration suppression. This is in agreement with previous work of the authors [23] demonstrating the same for white-noise excited lightly damped (i.e., non-isolated) structures.

Still, response parameters d_T and d_{TI} in Figures 4(c) and 4(d) do not exhibit any well-defined minimum on the ν-ξ_T plane: they monotonically decrease for higher TMDI frequency and damping ratios at a relatively fast rate (especially the TMDI stroke). The latter observation suggests that special care needs to be exercised in practical design of TMDI-equipped BISs in quantifying secondary mass clearance and stroke demands allowing for sufficient leeway to accommodate potentially perturbed ν and ξ_T values from the optimal ones.

3.2 | Performance assessment of white noise excited BIS+TMDIs for different TMDI inertial properties

In this section, performance and properties of EDI-optimal BIS+TMDIs are presented and discussed for different TMDI inertial propertiesfor a typical/reference BIS with T_I=3s and ξ_I=0.15. Secondary mass and inertance ratios are let to vary within μ= [0, 0.2] and β= [0, 1] intervals in $\mathbf{u}_2$ in Eq.(18) to include the limiting cases of BIS+TMD ($\mathbf{u}_2$=[μ 0]^T) and of BIS+TID ($\mathbf{u}_2$=[0 β]^T) as well as to address BISs with relatively low mass, such as sensitive equipment and artefacts housed in buildings, for which the upper limit of μ=0.2 and/or β=1 are practically feasible. To facilitate comparison between the effects of μ and β properties to EDI-optimal systems, results are plotted on the μ-β *inertial design plane* using iso-value curves in Figures 5 to 8. In these Figures, the origin

corresponds to the reference uncontrolled BIS, the y-axis to BIS+TMD (β=0) systems, the x-axis to BISs+TID (μ=0) systems, and any other point to BIS+TMDI systems.

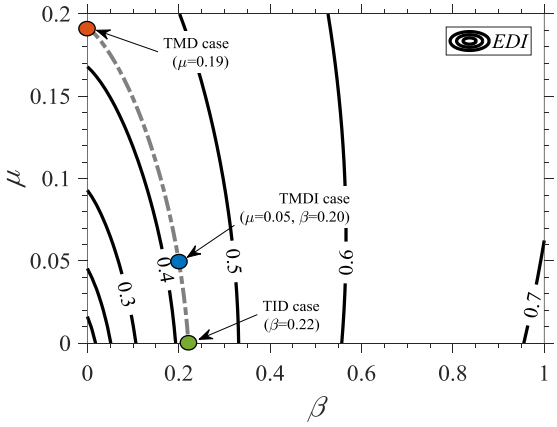

FIGURE 5 Optimal iso-value EDI index curves on the μ-β TMDI inertial design plane for white noise excited BIS with $\xi_I = 0.15$.

Figure 5 plots EDI on the μ-β plane. It is seen that, for *any* fixed μ value, EDI increases monotonically with β demonstrating that through EDI-based tuning increased inertance leads to larger input seismic energy being dissipated at the inertial damper than at the isolation layer regardless of the secondary mass ratio μ. Still, the rate of increase of EDI with β saturates fast suggesting that inerters with lower inertance are more efficient in diverting energy dissipation from the isolation layer to the inertial damper. On the other hand, it is seen that EDI increases appreciably with μ only for relatively low fixed β values, i.e., 0<β<0.3. For larger inertance values, EDI becomes less sensititve to increasing μ (iso-EDI curves run almost parallel to the y-axis), while for β>0.8 increasing μ is detrimental to EDI. From a *performance-based design* viewpoint, EDI iso-value curves suggest that the inclusion of a grounded inerter to a TMD-equipped BIS reduces considerably the overall mass/weight of the inertial damper required to achieve a target EDI performance. To quantify this practically important effect of the grounded inerter, three particular designs are considered in Figure 5 with common EDI= 0.42: a large-mass TMD with secondary mass equal to 19% of the total BIS mass, a TID with relatively large inertance equal to 22% of the total BISs mass, and a TMDI with inertance ratio β=20% and modest mass ratio μ=0.05, whose optimal EDI tuning has been previously discussed in detail (Figures 3 and 4). These indicative EDI-equivalent designs illustrate that a grounded inerter may achieve weight reduction of orders of magnitude compared to the classical (conventional) TMD. In fact, as the target EDI performance increases weight reduction achieved by the inerter becomes more and more dramatic justifying, eventually, the exclusive consideration of a TID (i.e., a theoretically massless inertial damper) with large inertance. Frequency response functions of the above three particular designs are provided in Figure A2 of the Appendix.

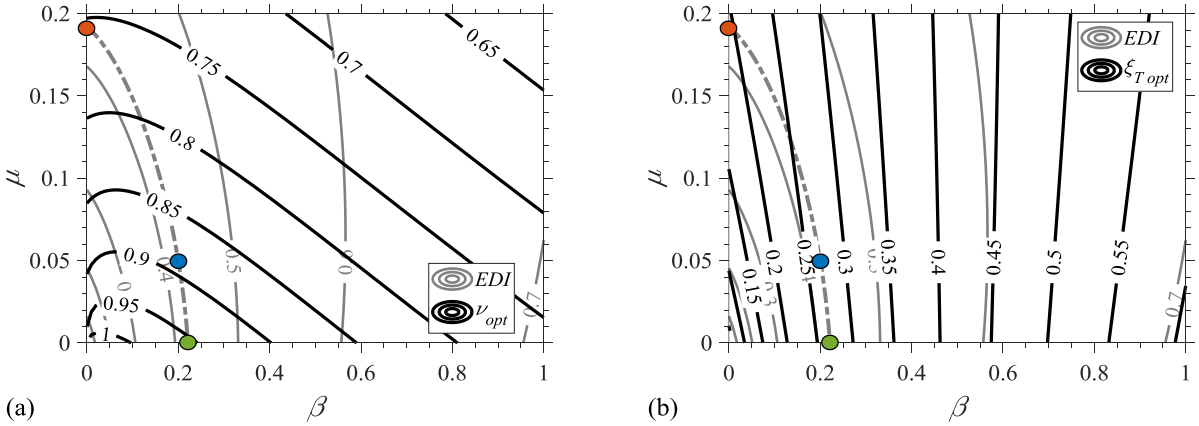

FIGURE 6 Optimal iso-value TMDI frequency ratio (a) and damping ratio (b) curves on the μ-β TMDI inertial design plane for white noise excited BIS with $\xi_I = 0.15$. EDI iso-value curves of Figure 5 are supersposed.

Figure 6 plots iso-value curves of the optimal TMDI frequency and damping ratio parameters, ν_{opt} and $\xi_{T\,\text{opt}}$, respectively, required to achieve the EDI values in Figure 5. The EDI iso-value curves of Figure 5 are superimposed. It is seen in Figure 6(a) that there is little correlation between optimal EDI and ν_{opt} iso-curves: the two families of iso-curves intersect at large angles. This observation suggests that careful TMDI frequency tuning is required for accurate performance-based EDI-optimal design regardless of μ andβ values. However, EDI and $\xi_{T\,\text{opt}}$ iso-value curves in Figure 6(b) are well-correlated especially for large inertance ratios (i.e., β>0.5) in which case they run in parallel. This observation suggests that increased EDI performance requires higher inertance and TMDI damping ratios simultaneously, while $\xi_{T\,\text{opt}}$ becomes insensitive to changes in μ. Focusing on the three previously discussed particular optimal designs with EDI=0.42 it is noted that whilst the difference in ν_{opt} between TID and TMDI is similar to the difference in their effective inertial ratio $\mu + \beta$ in Eq.(3) and equal to about 15%, their $\xi_{T\,\text{opt}}$ value is the same. On the antipode, a large difference to $\xi_{T\,\text{opt}}$ of more than 35% is observed between the TMDI and the TMD even though their effective inertial ratio difference is again of the order of 15% while ν_{opt} changes by only about 7%. These results demonstrate that $\xi_{T\,\text{opt}}$ is not sensitive to achieve a target EDI values for TMDIs with small secondary mass and large inertance ratio, while it becomes a critical design parameter for TMDIs with small inertance ratios.

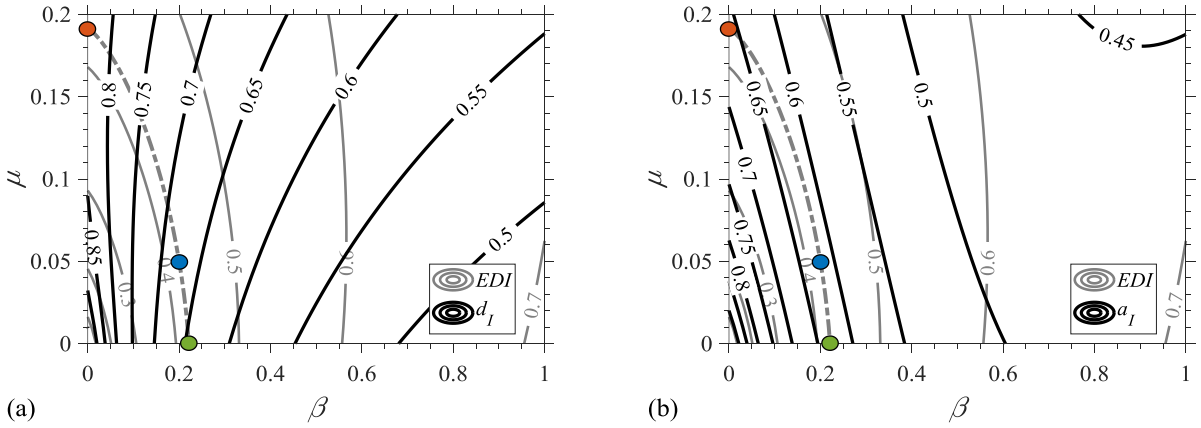

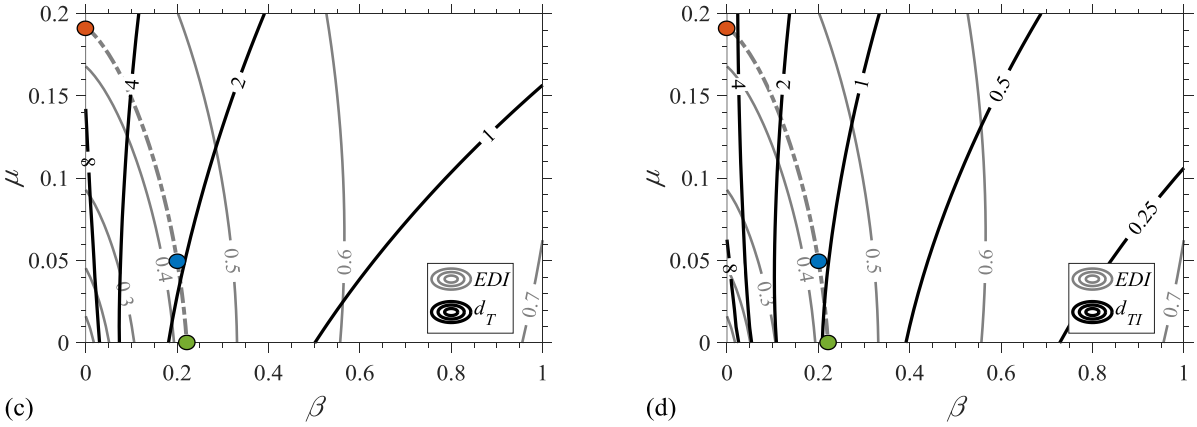

FIGURE 7 Optimal iso-value curves of performance indices in Eq.(14) on the μ-β TMDI inertial design plane for white noise excited BIS with ξ_I=0.15. EDI iso-value curves of Figure 5 are superposed.

Iso-value curves of all kinematic performance indices in Eq. (14) are plotted in Figure 7 together with EDI iso-value curves. Whilst there is discrepancy between the EDI and the d_I and a_I curves in Figures 7(a) and 7(b), respectively, *both* EDI-d_I *and* EDI-a_I iso-value curves observe similar trends for most of the inertance range considered (i.e., β<0.7). Specifically, similar to EDI, BISs displacement and total acceleration decrease *concurrently* with increasing β for any fixed μ value. More dramatic is the decrease of secondary mass displacement and, even more so, stroke demands with increasing β for any fixed μ value as seen in Figures 7(c) and 7(d), respectively. These reductions achieved by the inclusion of the grounded inerter are practically important, since secondary mass displacement and stroke of classical EDI-optimal TMDs are up to 8 times larger from the displacement of the uncontrolled BISs as seen in Figures 7(c) and 7(d), respectively (see also [15]). In general, for all four kinematics performance indices examined, higher performance improvement through increase of inertance is noted for EDI-optimal TMDI secondary system with relatively low effective inertial ratio $\mu + \beta$ since all iso-value curves in Figure 7 become denser as they approach the x-axis near the origin; as inertance increases for fixed μ its positive effects to all performance indices saturates. On the antipode, with the exception of BISs total acceleration, increasing μ for fixed β>0.1 (i.e., considering heavier TMDI with fixed inertance) is detrimental to all performance indices. Notably, similar trends on the performance of white noise base excited non-isolated structures equipped with TMDI optimally tuned for different criteria have been reported in the literature [22-23]. Practical consequences of these trends from a performance-based viewpoint can be appreciated by again examining the performance of the three previously considered TMD, TID, and TMDI secondary system designs attaining the same EDI=0.42 indicated on Figure 7. The TID achieves significant performance improvements compared to the large-mass TMD in terms of BIS displacement (more than 20% improvement), secondary mass displacement (about 6 times lower), and stroke (about 4 times lower). It further achieves 3.5% BIS displacement improvement compared to the considered lightweight TMDI and about 7% reduction to secondary mass displacement and stroke. Still, in terms of BIS total acceleration, the large-mass TMD and TID observe practically the same performance, while the TMDI improves performance by about 4%. Further insight on the comparative performance of the considered systems is gained by examining complex modal analysis results as well as frequency response functions provided in Figures A1 and A2 of the Appendix, respectively.

3.3 | Performance assessment of white noise excited BISs+TMDI for different isolation layer damping

This section examines the performance of white-noise excited EDI-optimal BIS+TMDI systems for different ξ_I damping values including, ξ_I= 0.01-0.05 (lightly damped BISs), ξ_I= 0.1-015 (high

damped BISs, reference primary system), and ξ_I = 0.30 (heavily damped BISs). Figure 8 plots performance indices in Eqs.(14) and (16) for the above ξ_I values as a function of the inertance ratio and for three different mass ratios: μ=0 (TID), μ=0.05 (lightweight TMD/TMDI), and μ=0.20 (large-mass TMD/TMDI). Performance ordinates on the y-axes of the left column of panels in Figure 8 correspond to uncontrolled BISs , while performance ordinates on the y-axes in the rest of the panels correspond to BISs+TMD with μ=0.05 and μ=0.20, respectively.

EDI performance curves plotted in the first row of panels in Figure 8 confirm that higher inertance ratio increases energy dissipation at the inertial damper, as previously discussed,and further show that the amount of this energy is heavily leveraged by ξ_I. Specifically, EDI decreases monotonically with increasing ξ_I for fixed effective TMDI inertial ratio suggesting that by increasing ξ_I a larger fraction of the total energy absorbed is dissipated at the isolation layer. Moreover, lower damping ratio ξ_I leads to faster saturation of EDI with increasing β as well as higher peak EDI limiting value. Lastly, TMDI secondary systems with large mass ratio μ attain significantly higher EDI in the region of low inertance ratios and for high ξ_I, but the effect of μ to EDI becomes less significant with increasing β.

BIS displacement, d_I, and absolute acceleration, a_I, plotted in the second and third panel rows in Figure 8, respectively, observe similar trends. They decrease monotonically as β and/or ξ_I increases but at increasingly smaller rates: the addition of a grounded inerter is more effective to suppress BIS displacement and acceleration for lower inertance and BIS damping ratios. In fact, the heavily damped BIS (ξ_I = 0.30) observes only marginal improvement in mitigating d_I and, even, small deterioration in a_I performance for β>0.4. Consideration of heavier TMDI (i.e., of increasing μ) reduces significantly BIS displacement and absolute acceleration for low inertance ratios and BISs damping, but its beneficial effect saturates as β and/or ξ_I increases. Lastly, d_I and a_I curves asymptotically coincide as β increases which signifies that for large β, the potential for BIS motion suppression is independent of ξ_I.

Turning attention to the secondary mass motion, it is seen in the last two panel rows of Figure 8 that the presence of a grounded inerter with increasing β reduces dramatically both the secondary mass displacement, d_T, and stroke, d_{TI}. These reductions are more prominent but also saturate faster with increasing BISs damping ratio higher ξ_I. Further, for EDI-optimal BIS+TMDI with different ξ_I, the d_T and d_{TI} do not coincide, as is largely the case for d_I and even more so for a_I, but rather they take on smaller values for higher ξ_I. Lastly, the effect of increasing the attached mass ratio μ is detrimental to d_T and d_{TI} especially for smaller inertance ratios β. Overall, numerical data in Figure 8 suggest that β can be traded for ξ_I and *vice versa* in meeting any particular fixed performance of the overall EDI-optimal BIS+TMDI.

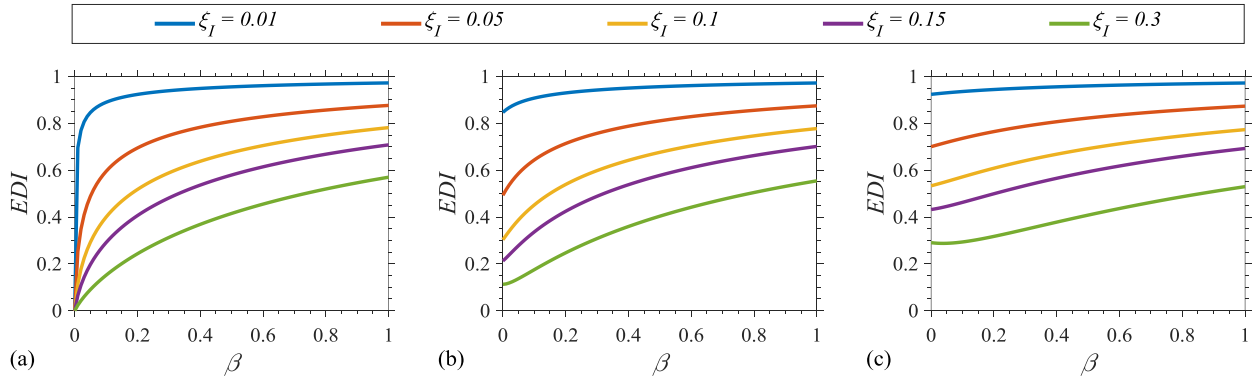

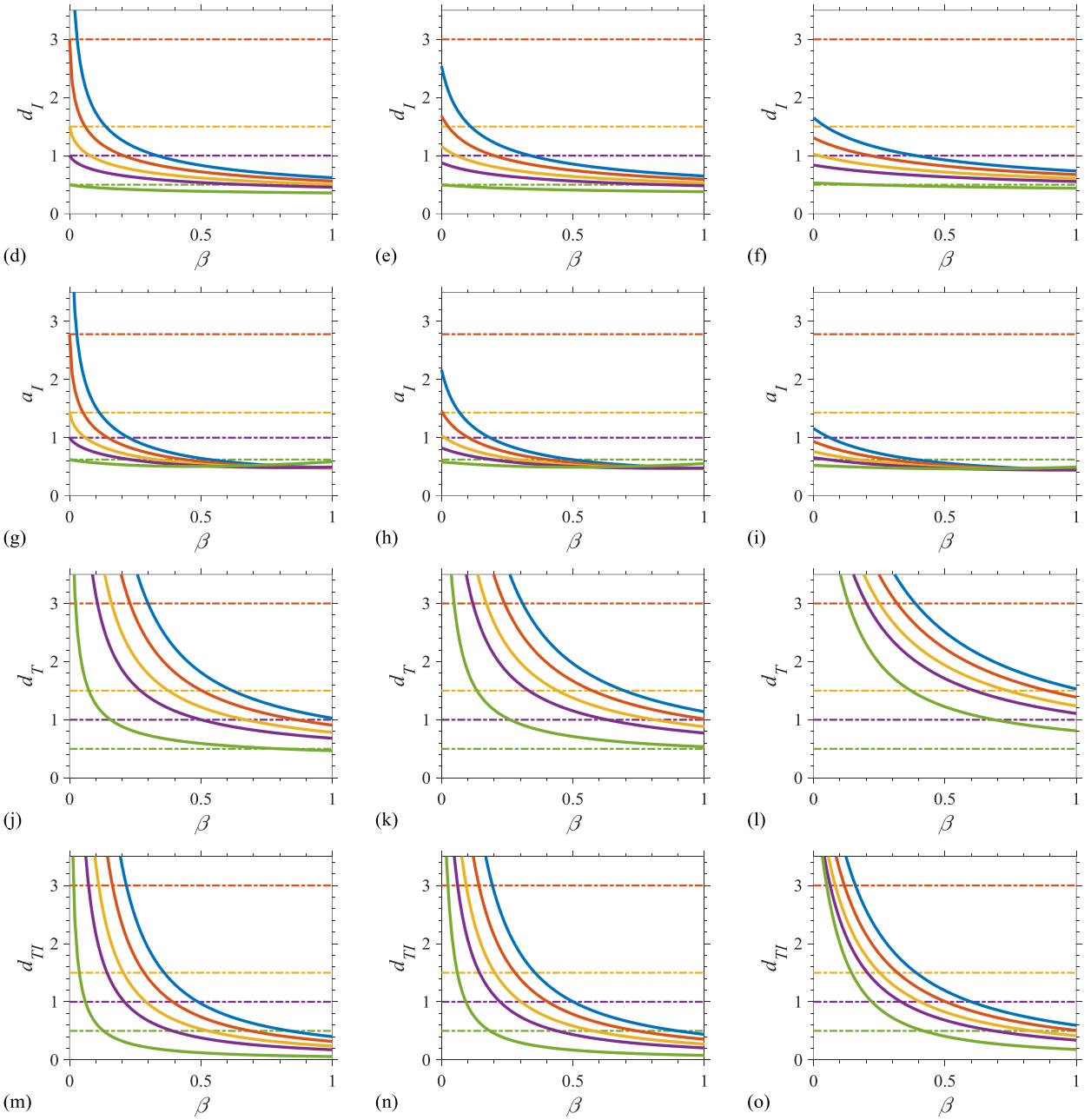

FIGURE 8 Performance of white-noise excited EDI-optimal BIS+TMDI systems as function of inertance ratio β for various BIS damping ratios ξ_I and mass ratios μ.

4 | PERFORMANCE ASSESSMENT OF OPTIMAL TMDI+BIS SYSTEMS FOR NON-WHITE EXCITATION

In the previous section EDI-optimal TMDI tuning was pursued assuming white noise input which is considered to be sufficient for designing flexible TMD-equipped BISs [14]. Nevertheless, the average frequency content of the earthquake-induced support excitation in BISs is non-white: for BISs resting on the ground, the frequency content of the seismic excitation depends heavily on local site conditions, while for BISs housed within structures it depends on the dynamical properties of the hosting structure. In this respect, this section focuses on assessing the performance of EDI-optimal TMDI+BIS systems designed for white noise input under colored noise and under recordered strong motion excitations.

4.1 | Stochastic colored noise excitation

Two different colored noise excitations are considered representing base excitations with high and low time-averaged frequency content. The excitations are modelled by the filtered Kanai-Tajimi spectrum in Eq. (9) with parameters ω_g= 10.73rad/s, ζ_g= 0.78, ω_f = 2.33rad/s and ζ_f= 0.90 for high frequency content, and ω_g= 5.34rad/s, ζ_g= 0.88, ω_f = 2.12rad/s and ζ_f= 1.17 for low frequency content as shown in Figure 9. These parameters were derived in [40] by fitting the spectrum of Eq.(9) to elastic response spectra used for code-compliant seismic design of structures founded on stiff sand (high input frequency content) and on soft clay (low input frequency content).

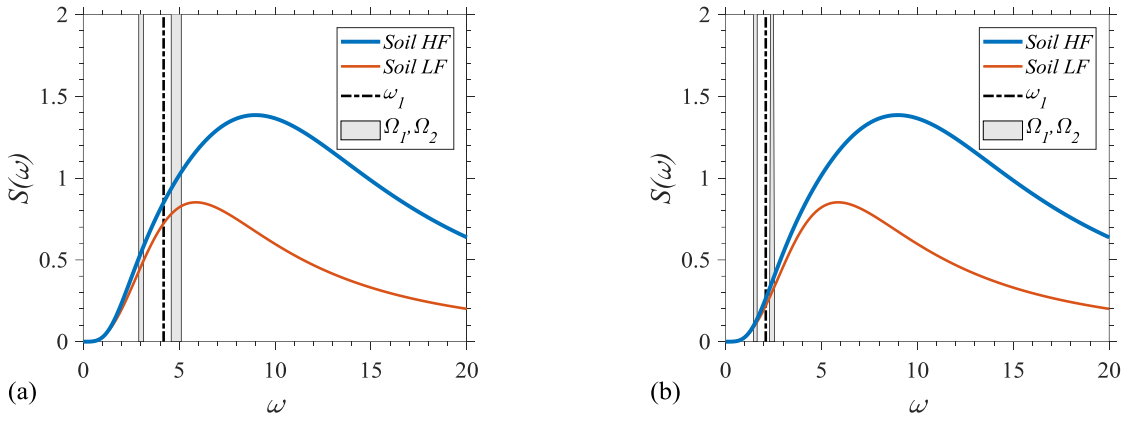

FIGURE 9 Colored noise spectra of different frequency content and natural frequencies of uncontrolled BISs and EDI-optimal TMDI+BISs systems with $\xi_I = 0.15$ and (a) $T_I = 1.5$ s, (b) $T_I = 3$ s.

Figure 10 plots iso-value curves on the μ-β plane for EDI and for the four kinematic performance indices in Eq.(14) obtained from white-noise EDI-optimal designed TMDI+BIS systems subject to the colored noise excitations of Figure 9. Results for a relatively stiff TMDI-equipped BIS with T_I=1.5s (i.e., ω_1=4.19 rad/s) and $\xi_I = 0.15$ as well as for the reference (flexible) TMDI-equipped BIS considered in Section 3.2 with T_I=3s (i.e., ω_1=2.09 rad/s) and $\xi_I = 0.15$ are presented in the left and in the right panel columns of Figure 10, respectively. Iso-value curves for white noise excitation are superposed in all panels of Figure 10 to enable comparisons between white and colored noise excitation. It is seen from the first row of panels in Figure 10, that the frequency content of colored excitations has negligible effect to EDI for the flexible TMDI-equipped BIS, while it does influence EDI values of the stiff TMDI-equipped BIS especially in the region of β<0.4. It is also seen that increasing the secondary mass ratio μ is always detrimental to EDI for colored noise excitation. However, increasing μ reduces the displacement index d_I for both considered colored noise excitations, for β<0.3 and for the stiffer TMDI-equipped BIS. Further, white-noise EDI-optimal TMDI for given μ and β ratios is more effective in controlling lateral sway BIS demands for the low frequency excitation compared to the high frequency excitation, especially for the stiffer BIS. This is attributed to the fact that the natural frequency of the stiff BIS is the closest to the dominant frequency of the low frequency colored noise excitation (see Figure 9).

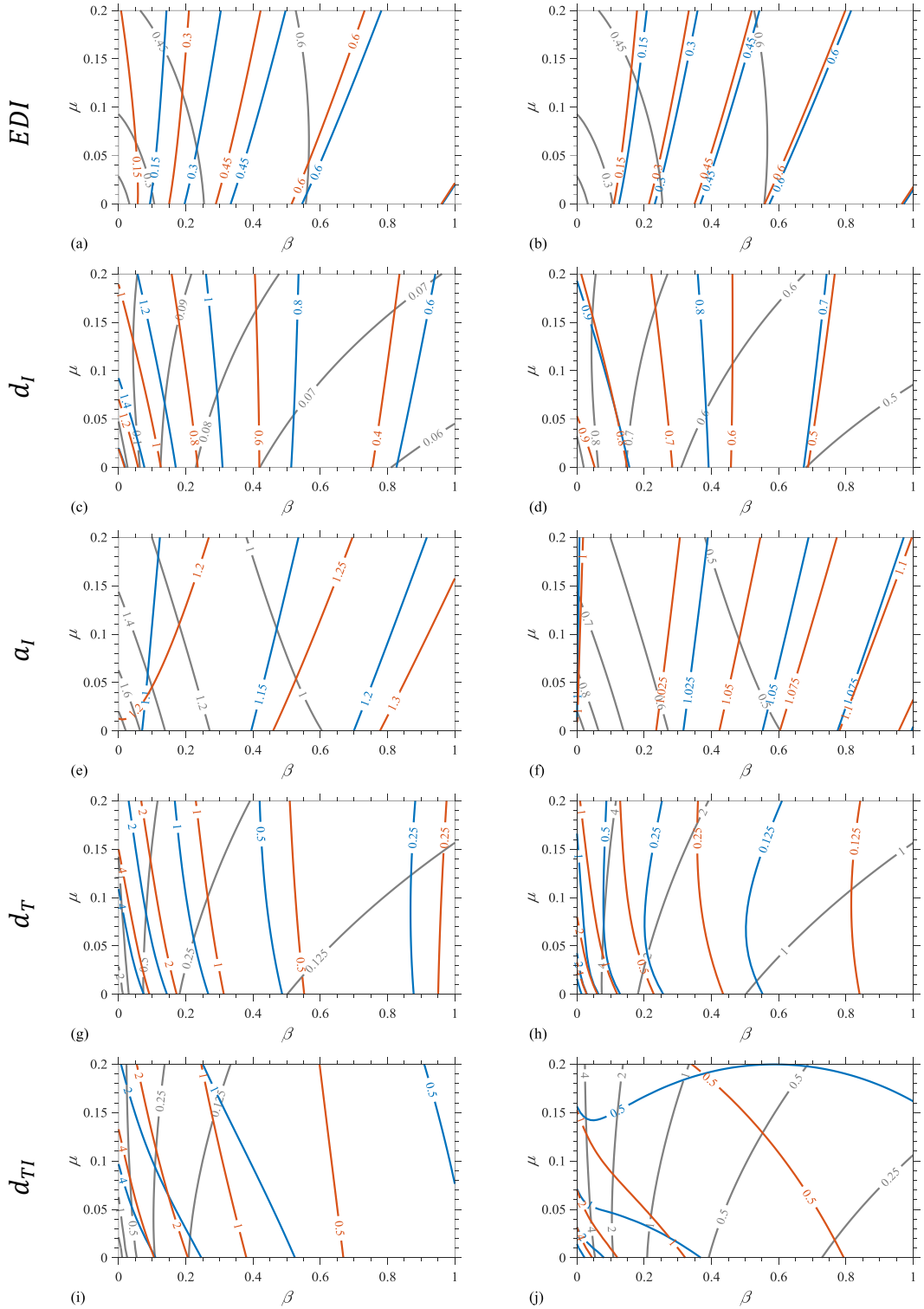

FIGURE 10 Iso-value curves of performance indices in Eq.(14) on the μ-β plane for white noise EDI-optimal BIS+TMDI systems with $T_I = 1.5$ s (left column) and $T_I = 3$ s (right column) and $\xi_I = 0.15$ exposed to colored noise spectra of Figure 5.

It, therefore, becomes evident that white-noise EDI-optimal TMDIs become more effective for mitigating displacement of the base isolation layer as the average dominant frequency of the seismic input motion lies closer to the effective natural frequency of the uncontrolled BIS. This is a quite positive finding from a practical viewpoint as it addresses the challenging combination of flexible or stiff BISs resting on similarly flexible or stiff supporting conditions, respectively.

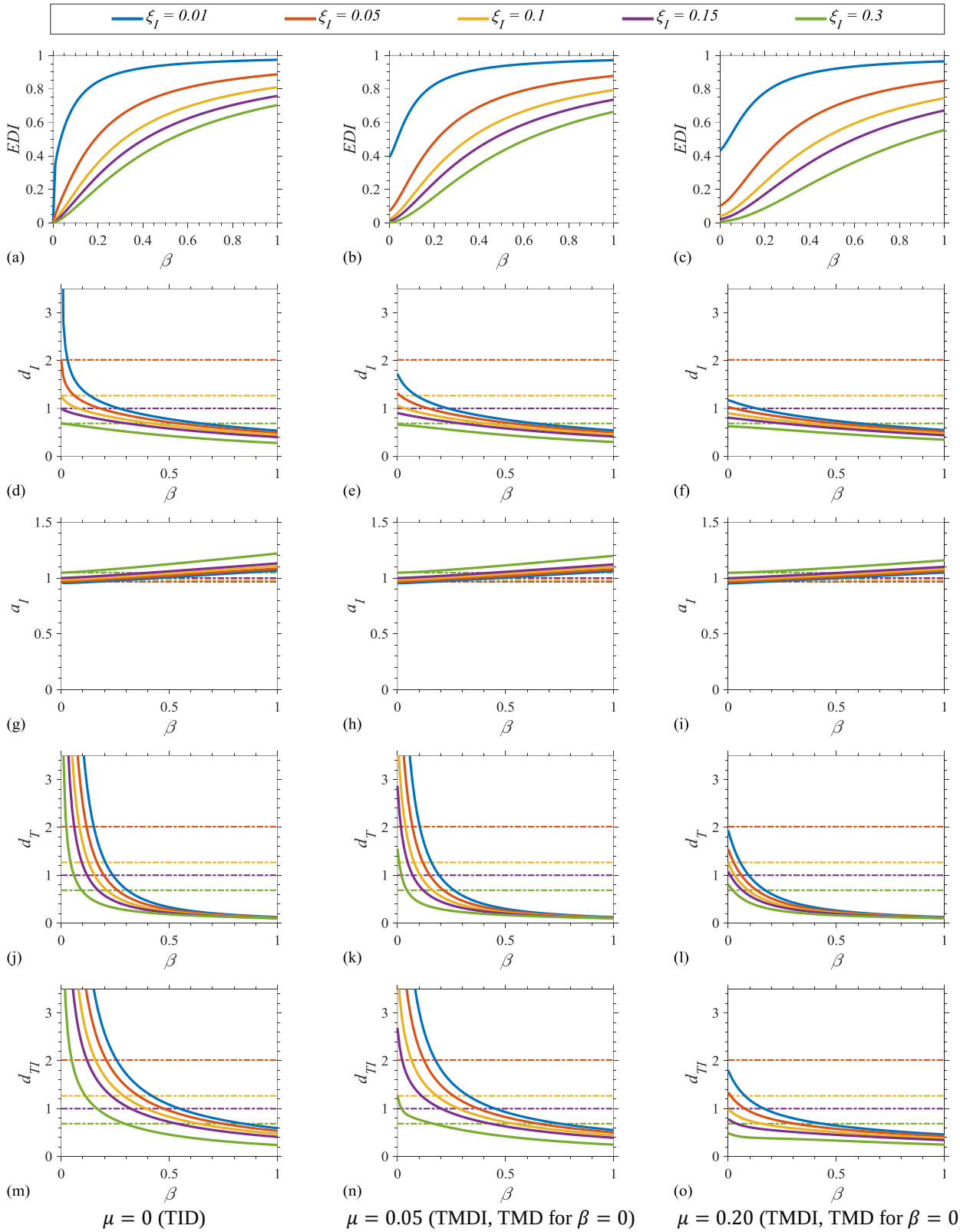

FIGURE 11 Performance of white-noise excited EDI-optimal BIS+TMDI systems for low frequency colored noise excitation in Figure 5 as function of inertance ratio β for various BIS damping ratios ξ_I and mass ratios μ and for $T_I = 3$ s.

Further examination of the d_I iso-value curves for fixed μ values shows that BIS lateral displacement reduces significantly and monotically at increasing β for both colored noise excitations as in the case of white noise excitation. Nevertheless, the opposite trend is noted for the BIS

acceleration performance index a_I. This performance deterioration trend with β is more pronounced for the stiff TMDI-equipped BIS and for the low frequency content excitation. This trend is readily justified by comparing the dominant frequency of the colored noise spectral shapes in Figure 9 with the second (higher) pseudo-frequency, Ω_2, of white-noise EDI-optimal TMDI-equipped BISs which corresponds to the second vibration mode associated with faster dynamics, hence, influencing mostly the acceleration response. To this effect, note that Ω_2 increases with increasing β as seen in Figure A1(b) for the case of the reference/flexible TMDI-equipped BIS (similar trends apply for the stiff BIS+TMDI systems), and therefore approaches from the left the dominant frequency of the colored noise spectra. This is pictorially shown in Figure 9 where the range of Ω_2 is depicted for the three particular white-noise EDI-optimal TMDI-equipped BIS systems reported in Table A1. The Ω_2 pseudo-frequency of the stiff BIS practically coincides with the dominant frequency of the low frequency colored noise resulting in increasing BIS acceleration demands represented by performance index a_I.

Turning the attention to the secondary mass RMS displacement d_T, similar trends for the two different colored noise excitations are noted for both BISs considered: the effect of increasing inertance ratio β is beneficial for any fixed mass ratio μ value, while TMDI+BIS systems with a small mass ratio μ<0.05 perform slightly better than TID+BIS systems across the board. Lastly, secondary mass RMS stroke d_{TI} index for the stiff BIS reduces significantly with increasing β for any fixed mass ratio μ value for both colored noise excitations and this is is also the case with increasing of μ, contrary to what is observed for white noise excitation for which increasing μ is detrimental to the stroke. However, the stroke index d_{TI} for the flexible BIS becomes sensitive to high frequency input excitation for the relatively heavy TMDIs while for lightweight (μ<0.05) TMDIs, increasing of both β and μ ratios reduce secondary mass stroke demands regardless of the excitation frequency content.

Next, Figure 11 plots performance indices for the low frequency content colored noise as a function of the inertance ratio β and for the same reference BIS system, attached mass ratios μ, and damping values ξ_I previously considered in Figure 8. Overall, it is seen that, with the exception of the BIS acceleration performance index a_I, performance follows the same positive trends with increasing βas in the case of white noise excitation in Figure 8. However, the increase of inertance *and* of BIS damping is detrimental to the BIS acceleration for colored noise excitation though this increase is insignificant for lightly damped BISs and lightweight TMDIs compared to reductions to BIS displacement demands with increasing β.

As a closure to this section, note that same trends as in Figure 11 are found for the high frequency colored noise excitation and for the stiff BIS and therefore including further numerical results for the above case is deemed redundant.

4.2 | Recorded strong ground motion excitation

Acceleration traces of ground motion (GMs) recorded during historic seismic events attain time-varying amplitude and frequency content. Such non-stationary excitation attributes affects the effectiveness of TMDs for vibration mitigation of BISs, especially in terms of peak response, as there may not be sufficient time, in terms of cycles of response, for kinetic energy to be transferred from the flexible BIS to the secondary mass (see e.g., [12-14]). Therefore, it is deemed important to further assess the performance of different TMDI-equipped BIS systems to recorded GMs with different time-varying attibutes. To this aim, the four GMs listed in Table 2 are chosen to conduct response history analysis to the uncontrolled reference BIS (T_I=3s and $\xi_I = 0.15$) previously examined as well as to the same BIS equipped with three different inertial dampers EDI-optimally designed to stationary white-noise excitation (values of optimal parameters, natural psedo-frequencies, psedo-periods and pseudo-damping are reported in the Appendix): the TMDI indicated in Figure 5 with mass ratio μ=0.05 and inertance ratio β=0.2, a TMD with same mass μ=0.05 as the TMDI, and a TID with same inertance β=0.2 as the TMDI. The focus herein is on evaluating the effects of the grounded inerter to the TMD-equipped BIS as well as of the attached mass to the TMDI-equipped BIS for the

chosen recorded GM signals whose frequency domain attributes are described in the last column of Table 2.

TABLE 2 Recorded acceleration ground motions considered in the TMDI+BIS system performance assessment

Event	Magnitude	GM record station	Peak ground acceleration [g]	Attributes
Imperial Valley, CA (1940)	7.0	El Centro Array # 9	0.315	Near-fault pulse-free GM rich in high frequencies
Tokachi-Oki, Japan (1968)	7.9	Hachinohe	0.229	Far-field broadband GM with significant energy at 3s period
Irpinia, Italy (1980)	6.9	Sturno	0.232	Near-fault GM with pulse of period 3.1s late in time
Kobe, Japan (1995)	6.9	KJMA	0.345	Near-fault GM with pulse of period 1s early in time

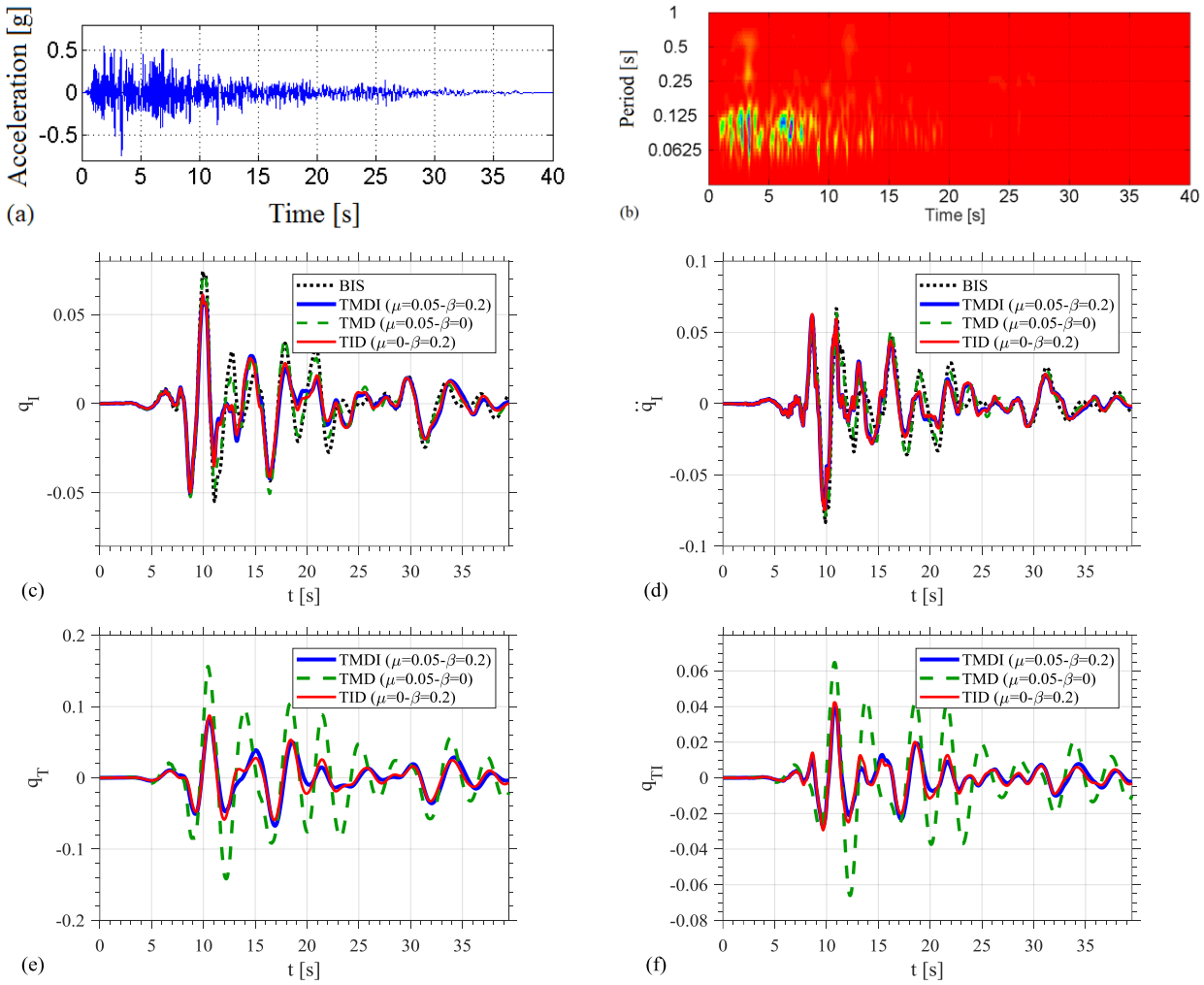

FIGURE 12 El Centro array #9 ground motion and normalized response-history analysis results (a) input time-history (b) wavelet-based energy distribution of input time-history on natural period-time plane (c) BIS displacement response (d) BIS acceleration response (e) secondary mass displacement response (f) secondary mass stroke response.

Time traces of the four GMs of Table 2 are plotted in the upper left panel in Figures 12-15. Corresponding contour plots of the GM energy distribution on the time-natural period plane are provided in the upper right panel in Figures 12-15. In these plots the time-varying GM frequency composition is traced in terms of period $T=2\pi/\omega$ with colder colors indicating more dominant (i.e., higher amplitude) frequency components. The plots are obtained from standard GM wavelet

transform analysis (see e.g., [41-42] and references therein) and are herein used to inform the attributes of the considered GMs in Table 2 and to facilitate structural response results interpretation. The rest of the panels in Figures 12-15 plot response time-histories of all considered structural systems in terms of BIS normalized displacement, q_I, and acceleration, $\ddot{q}_I$, as well as secondary mass displacement, q_I, and stroke, q_{TI}.

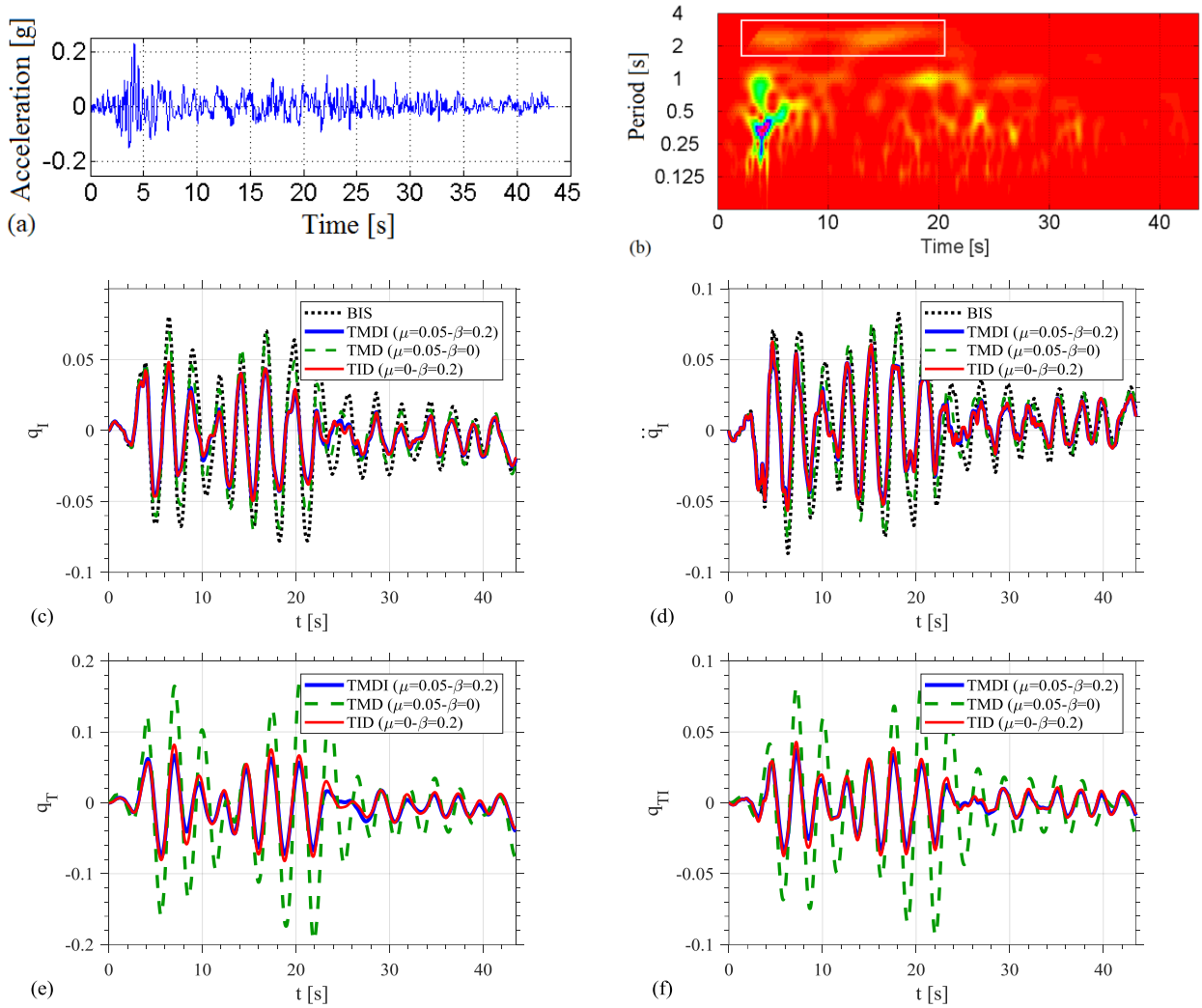

FIGURE 13 Hachinohe ground motion and normalized response-history analysis results (a) input time-history (b) wavelet-based energy distribution of input time-history on natural period-time plane (c) BIS displacement response (d) BIS acceleration response (e) secondary mass displacement response (f) secondary mass stroke response.

Commenting first on structural response results for the El Centro GM excitation whose narrow-band frequency content is centered well-away from the natural frequencies of all considered structural systems, it is seen that the incorporation of the grounded inerter reduces to some extent *both* BIS displacement *and* acceleration compared to the uncontrolled BIS and to the TMD-equipped BIS (Figure 12). Note that this was not the case for stationary high-frequency colored noise excitation for which BIS acceleration response increased with increasing inertance (see Figure 10). Further, significant reductions are achieved in terms of secondary mass motion.

Different from the previous GM, Hachinohe record is a typical broadband far-field GM previously considered for the assessment of benchmark controlled structures [43]. It features well-spread in time frequency content within the range of the natural periods of the examined structural systems as indicated on the wavelet contour plot in Figure 13(b) by a white window. These components result in a large number of response cycles with significant amplitude for the BIS. It is

seen that the grounded-inerter mass-dampers are much more efficient in reducing the amplitude of these cycles in terms of BIS displacement *and* acceleration compared to the conventional TMD. They also reduce by more than half the peak secondary mass displacement and stroke.

The Sturno GM has been chosen as a representative pulse-like near-fault GM as clasified in [44] having a pulse period close to the BIS natural period as indicated by a white window in Figure 14(b). The low-frequency (long period) pulse arrives in time after significant energy at much higher frequencies (shorter periods) has been released. This relatively late pulse arrival, which is typical of forward-directivity ground motion pulses (see [44] and references therein), allows time for mass-dampers to be activated andto contribute to BIS motion mitigation despite the impulsive nature of the input excitation. In this regard, the TMD does reduce BIS response displacement *and* acceleration but these reductions become much more significant with the incorporation of the inerter which, as before, reduces dramatically peak and RMS secondary mass motion.

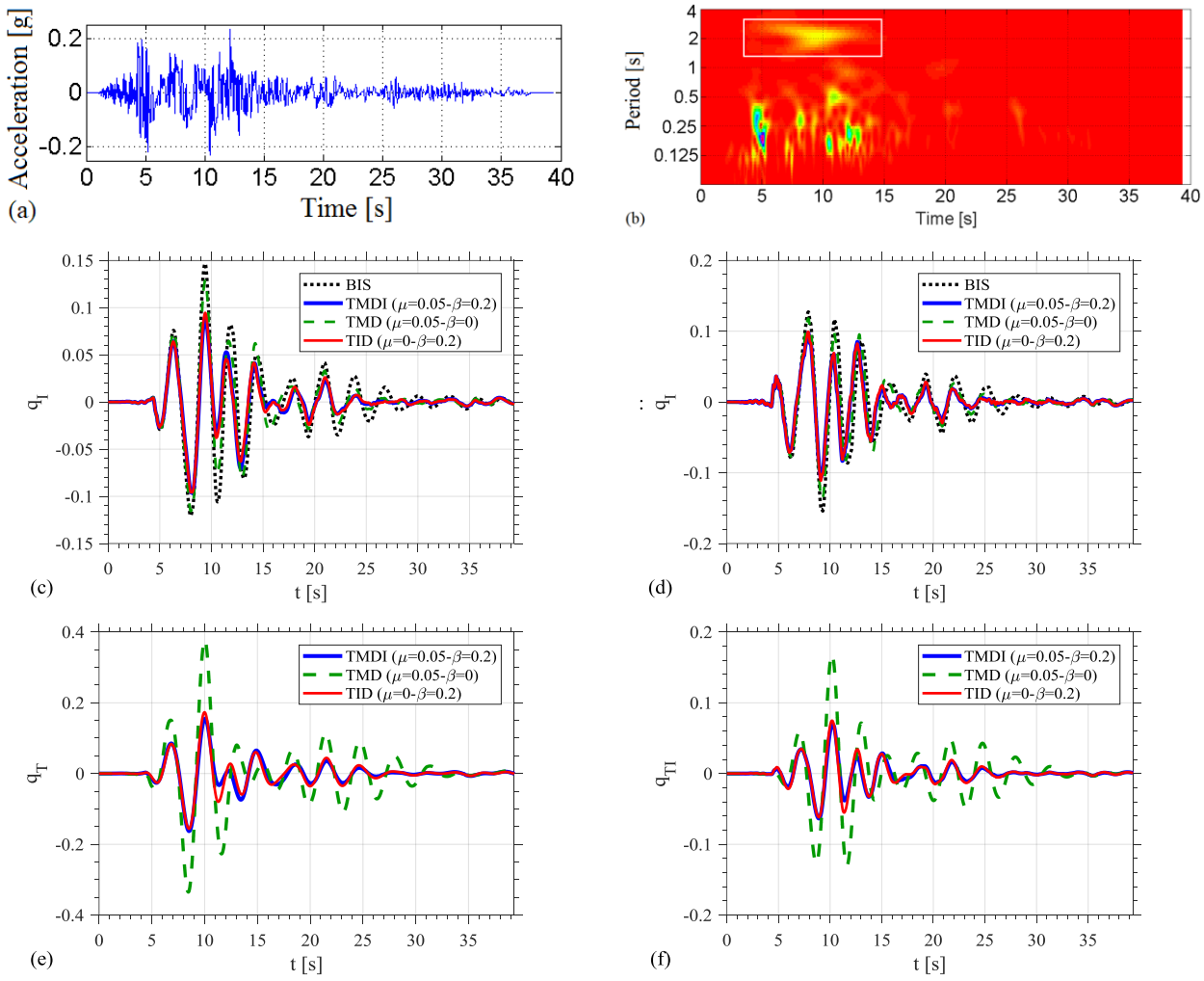

FIGURE 14 Irpinia-Sturno ground motion and normalized response-history analysis results (a) input time-history (b) wavelet-based energy distribution of input time-history on natural period-time plane (c) BIS displacement response (d) BIS acceleration response (e) secondary mass displacement response (f) secondary mass stroke response.

Lastly, the KJMA GM recorded during the Kobe (1995) earthquake at distance less than 1km from the fault is taken as the least benign excitation waveform as it is characterized by the very early arrival of relatively low-frequency pulses shown in Figure 15(b) (see also discussion in [14] who considered the same GM for TMD+BIS performance assessment). For this particular GM, all mass-dampers are ineffective for any significant peak BIS displacement reduction, though the grounded

inerter does achieve some RMS BIS displacement recuction. Further, mass-dampers actually increase BIS acceleration response and the inclusion of the inerter is detrimental along these lines as seen before for stationary colored noise excitation in Figure 10. Yet, the increase is not significant while, at the same time, the grounded inerter does achieve non-negligible reduction to secondary mass motion.

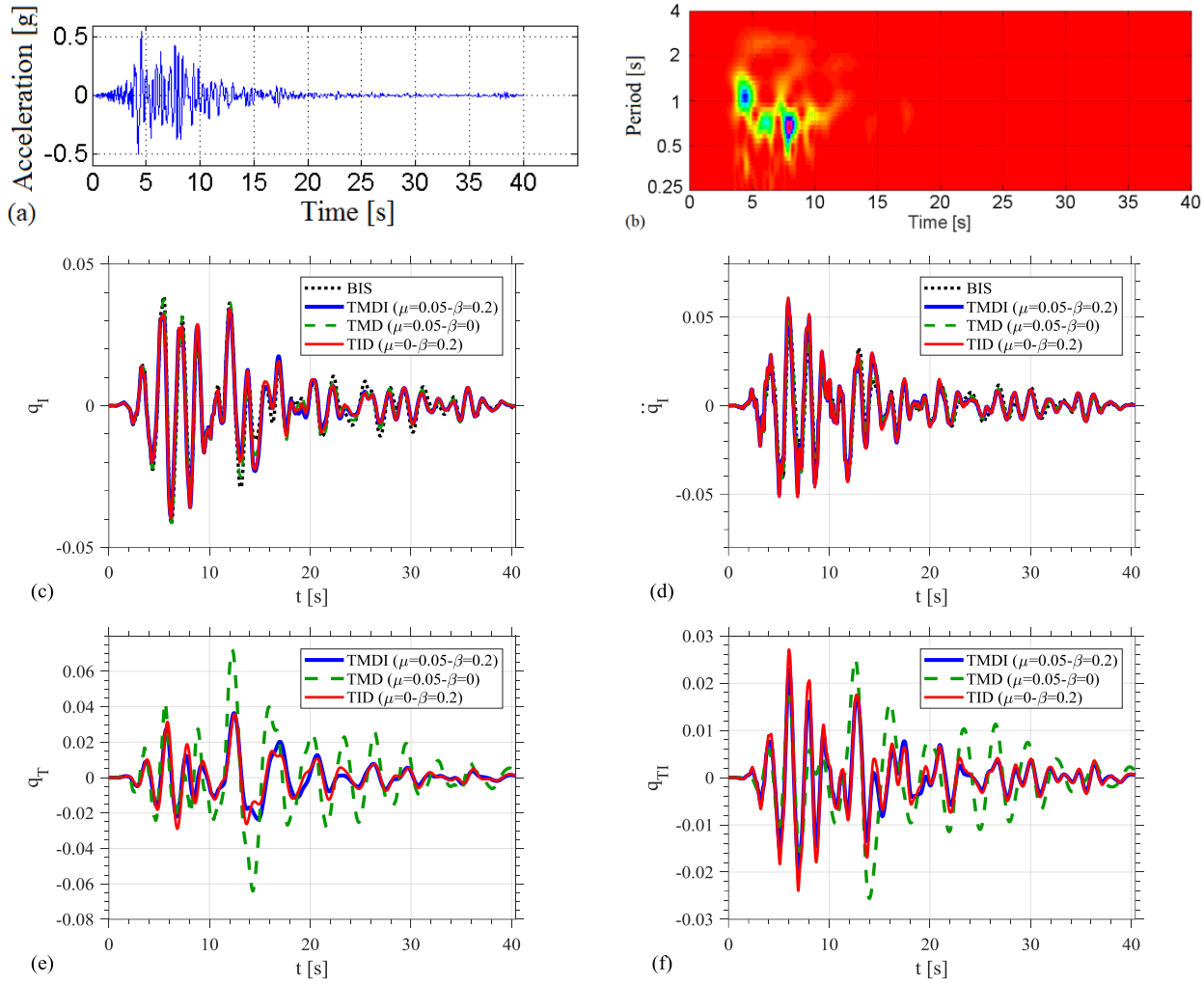

FIGURE 15 Kobe-KJMA ground motion and normalized response-history analysis results (a) input time-history (b) wavelet-based energy distribution of input time-history on natural period-time plane (c) BIS displacement response (d) BIS acceleration response (e) secondary mass displacement response (f) secondary mass stroke response.

Overall, results furnished in Figures 12-15 demonstrate that with the exception of some peculiar seismogenetic environments favouring the early arrival of low-frequency impulsive ground motion waveforms, white-noise EDI-optimally designed mass-dampers with grounded inerter reduce significantly BIS displacement *and* acceleration response to both far-field and near-field GMs. They further show insignificant difference to the performance of the TMDI and the TID suggesting that the TID is preferable being significantly lighter while, at the same time, the unavoidable existence of some mass/weight in a real-life inertial damper (TID is only ideally massless) will not incur any deterioration from TID performance as long as it is accounted for in EDI-optimal tuning.

5 | CONCLUDING REMARKS

In this work, the effectiveness of adding a grounded inerter to tuned mass dampers (TMDs) in reducing the lateral displacement of base isolated systems (BISs) without significantly increasing the accelerations is investigated. With the adopted models and range of values considered for secondary

mass and inertance, it has been possible to compare performances of (energy-based) optimized classical TMD configurations against optimal tuned mass damper inerter (TMDI) and tuned inerter damper (TID) for white noise (WN) excitation as well as for colored white noise (CWN) and for recorded seismic accelerograms. Focus was givem to different BISs ranging from isolated large-scale civil engineering structures (e.g., buildings or decks of bridges) to isolated sensitive secondary components and important artefacts housed within building structures.

As a general conclusion, the results demonstrated that adding the inerter leads to significant reduction of primary and secondary mass displacements, and of secondary mass stroke, all being important design constraints in conventional TMDs, while reduction of acceleration is simultaneously achieved for BISs characterized by low values of the BIS damping ratio, ξ_I.

In the case of WN base excitation it was found that:

- for fixed inertance ratios β, the TMDI and TID control systems have comparable performances: specifically, for mass ratio μ up to 0.2, and for β>0.3, the TID performs slightly better than the TMDI, while the opposite happens for β <0.3;
- the positive influence of the considered control systems (TMD, TMDI and TID) to BIS performances, gradually reduces by increasing ξ_I up to a limit value of ξ_I=0.3, beyond which an uncontrolled (heavily damped) BIS performs similarly with and without inertial/mass dampers.

In the case of CWN base excitation, the above trends under WN excitation have been confirmed: the inclusion of the inerter allows for reduction of BIS displacement being more significant as the ξ_I reduces, whilst causing moderate increase of BIS accelerations. In addition, it was shown that the inclusion of some secondary mass (i.e., TMDI as opposed to TID) achieves significant reduction to the kinematics of the inertial damper.

In the case of systems excited by recorded accelerograms, all previous observations made for WN and CWN excitations are confirmed for both near-fault and far-field earthquakes. Specifically, the grounded inerter is particularly effective in reducing the kinematics of the inertial damper even in the case of near-field accelerograms characterized by an early arrival of high energy content at low frequencies, even though, for the latter particular type of excitation, BIS displacement and acceleration demands were not mitigated compared to the uncontrolled structure

As a final remark, it is noted that throughout this work linear and ideal device behavior has been assumed. The authors are currently undertaking pertinent experimental work to explicitly account for the nonlinear behavior of isolators as well as of non-ideal behavior of inerter devices.

ACKNOWLEDGEMENTS

The financial support of Sapienza University of Rome under the Grant No. C26V16Z7YW for hosting Visiting Professors (financial framework 2016/2017), is gratefully acknowledged.

REFERENCES

[1] Kunde, M.C., R.S. Jangid, 2003: Seismic behavior of isolated bridges: a-state-of-the-art review. *Electronic Journal of Structural Engineering*, 3, 140–170.

[2] Warn, G.P. and K.L. Ryan, 2012: A review of seismic isolation for buildings: historical development and research needs. *Buildings*, 2, no. 3, 300–25.

[3] Reggio, A. and M. De Angelis, 2015: Optimal energy-based seismic design of non-conventional Tuned Mass Damper (TMD) implemented via inter-story isolation. *Earthquake Engineering and Structural Dynamics*, 44, no. 10, 1623–1642.

[4] De Angelis, M., R. Giannini and F. Paolacci, 2010: Experimental investigation on the seismic response of a steel liquid storage tank equipped with floating roof by shaking table tests. *Earthquake Engineering and Structural Dynamics*, 39, no. 4, 377–396, doi:10.1002/eqe.945.

[5] Paolacci, F., R. Giannini, and M. De Angelis, 2013: Seismic response mitigation of chemical plant components by passive control techniques. *Journal of loss prevention in the process industries*, 26, no.5, 924–935.

[6] Whittaker, A.S., M. Kumar and M. Kumar, 2014: Seismic isolation of nuclear power plants. *Nuclear Engineering Technology*, 46, no. 5, 569–580.

[7] Reggio, A. and M. De Angelis, 2014: Optimal design of an equipment isolation system with nonlinear hysteretic behaviour. *Earthquake Engineering and Structural Dynamics*, 42, no. 13, 1907–1930, doi:10.1002/eqe.2304.

[8] Reggio, A. and M. De Angelis, 2014: Combined primary–secondary system approach to the design of an equipment isolation system with High-Damping Rubber Bearings. *Journal of Sound and Vibration*, 333, no. 9, 2386–2403.

[9] Jangid, R.S. and J.M. Kelly, 2001: Base isolation for near-fault motions. *Earthquake Engineering and Structural Dynamics*, 30, no. 5, 691–707.

[10] Kelly, J.M., 1999: The role of damping in seismic isolation. *Earthquake Engineering and Structural Dynamics*, 28, no. 1, 3–20.

[11] Yang, J.N., A. Danielians and S.C. Liu, 1991: Aseismic hybrid control systems for building structures.
Journal of Engineering Mechanics, 117, no. 4, 836–853.

[12] Tsai, H.C., 1995: The effect of tuned-mass dampers on the seismic response of base-isolated structures. *International Journal of Solids and Structures*, 32, no. 8–9, 1195–1210.

[13] Palazzo, B., L. Petti and M. De Ligio, 1997: Response of base isolated systems equipped with tuned mass dampers to random excitations. *Journal of Structural Control*, 4, no. 1, 9–22.

[14] Hoang, N., Y. Fujino and P. Warnitchai, 2008: Optimal tuned mass damper for seismic applications and practical design formulas. *Engineering Structures*, 30, no. 3, 707–715.

[15] Taniguchi, T., A. Der Kiureghian and M. Melkumyan, 2008: Effect of tuned mass damper on displacement demand of base-isolated structures. *Engineering Structures*, 30, no. 12, 3478–3488.

[16] Petti, L., G. Giovanni, M. De Luliis and B. Palazzo, 2010: Small scale experimental testing to verify the effectiveness of the base isolation and tuned mass dampers combined control strategy. *Smart Structures and Systems*, 6, no. 1, 57–72.

[17] Den Hartog, J.P., 1956: *Mechanical Vibrations. 4th ed.* McGraw-Hill, New York.

[18] De Angelis, M., S. Perno and A. Reggio, 2012: Dynamic response and optimal design of structures with large mass ratio TMD. *Earthquake Engineering and Structural Dynamics*, 41, no. 1, 41-60.

[19] Smith, M.C., 2002: Synthesis of mechanical networks: the inerter. *IEEE Transactions on Automatic Control*, 47, no. 10, 1648–1662.

[20] Saitoh, M., 2012: On the performance of gyro-mass devices for displacement mitigation in base isolation systems. *Structural Control and Health Monitoring*, 19, no. 2, 246–259.

[21] Marian, L. and A. Giaralis, 2014: Optimal design of a novel tuned mass-damper-inerter (TMDI) passive vibration control configuration for stochastically support-excited structural systems. *Probabilistic Engineering Mechanics*, 38, 156–164.

[22] Marian, L. and A. Giaralis, 2017: The tuned mass-damper-inerter for harmonic vibrations suppression, attached mass reduction, and energy harvesting. *Smart Structures and Systems*, 19, no. 6, 665–678.

[23] Pietrosanti, D., M. De Angelis and M. Basili, 2017: Optimal design and performance evaluation of systems with Tuned Mass Damper Inerter (TMDI). *Earthquake Engineering and Structural Dynamics*, 46, no. 8, 1367–1388, doi:10.1002/eqe.2861.

[24] Lazar, I.F., S.A. Neild and D.J. Wagg, 2014: Using an inerter-based device for structural vibration suppression. *Earthquake Engineering and Structural Dynamics*, 43, no. 8, 1129–1147.

[25] Giaralis, A. and A. Taflanidis, 2018: Optimal tuned mass-damper-inerter (TMDI) design for seismically excited MDOF structures with model uncertainties based on reliability criteria. *Structural Control and Health Monitoring*, 25, no. 2, e2082.

[26] Zhao, C., J. Kikuchi, M. Ikenaga, K. Ikago and N. Inoue, 2016: Viscoelastically supported viscous mass damper incorporated into a seismic isolation system. *Journal of Earthquake and Tsunami*, 10, no. 3, 1640009.

[27] Zhang, Y. and W.D. Iwan, 2002: Protecting base-isolated structures from near-field ground motion by tuned interaction damper. *Journal of Engineering Mechanics*, 128, no. 3, 287–295.

[28] Saito, K., K. Yogo, Y. Sugimura, S. Nakaminami and K. Park, August 2004: Application of rotary inertia to displacement reduction for vibration control system. *13th World Conference on Earthquake Engineering*, 13, no. 1764.

[29] Xiang, P. and A. Nishitani, 2014: Optimum design for more effective tuned mass damper system and its application to base-isolated buildings. *Structural Control and Health Monitoring*, 21, no. 1, 98–114.

[30] De Domenico, D. and G. Ricciardi, 2018: An enhanced base isolation system equipped with optimal tuned mass damper inerter (TMDI). *Earthquake Engineering and Structural Dynamics*, 47, no. 4, 1169-1192.

[31] Dicleli, M. and S. Buddaram, 2007: Comprehensive evaluation of equivalent linear analysis method for seismic-isolated structures represented by SDOF systems. *Engineering Structures*, 29, no. 8, 1653–1663.

[32] Sayani, P. and K. Ryan, 2009: Evaluation of approaches to characterize seismic isolation systems for design. *Journal of Earthquake Engineering*, 13, no. 6, 835–851.

[33] Bhagat, S. and A.C. Wijeyewickrema, 2017: Seismic response evaluation of base-isolated reinforced concrete buildings under bidirectional excitation. *Earthquake Engineering and Engineering Vibration*, 16, no. 2, 365–382.

[34] Yenidogan, C. and M. Erdik, 2016. A comparative evaluation of design provisions for seismically isolated buildings. *Soil Dynamics and Earthquake Engineering*, 90, 265–286.

[35] Jara, J.M., G. Raya, B.A. Olmos and G. Martinez, 2017: Applicability of equivalent linearization methods to irregular isolated bridges. *Engineering Structures*, 141, 495–511.

[36] Igusa, T. and A. Der Kiureghian, 1985: Dynamic characterization of two degree-of-freedom equipment-structure systems. *Journal of Engineering Mechanics*, 111, no. 1, 1–19.

[37] Lin, Y, 1967: *Probabilistic Theory of Structural Dynamics*. McGraw-Hill, New York.

[38] Clough, R.W. and J. Penzien, 1993: *Dynamics of structures*. McGraw-Hill, New York.

[39] Taflanidis, A.A. and J.T. Scruggs, 2010: Performance measures and optimal design of linear structural systems under stochastic stationary excitation. *Structural Safety*, 32, no. 5, 305-315.

[40] Giaralis, A. and P.D. Spanos, 2012: Derivation of response spectrum compatible non-stationary stochastic processes relying on Monte Carlo peak factor estimation. *Earthquakes and Structures*, 3, no. 3, 581–609.

[41] Torrence, C. and G.P. Compo, 1998: A Practical Guide to Wavelet Analysis. *Bulletin of the American Meteorological Society*, 79, no. 1, 61–78.

[42] Spanos, P.D., A. Giaralis, N.P. Politis and J.M. Roessett, 2007: Numerical treatment of seismic accelerograms and of inelastic seismic structural responses using harmonic wavelets. *Computer-Aided Civil and Infrastructure Engineering*, 22, no.4, 254–264.

De Angelis M, Giaralis A, Petrini F and Pietrosanti D. (2019) Optimal tuning and assessment of inertial dampers with grounded inerter for vibration control of seismically excited base-isolated systems. *Engineering Structures*, 196: 109250. DOI: 10.1016/j.engstruct.2019.05.091.

[43] Ohtori, Y., R.E. Christenson, B.F.J. Spencer and S.J. Dyke, 2004: Benchmark structural control problems for seismically excited nonlinear buildings. *Journal of Engineering Mechanics*, 130, no.4, 366–85.

[44] Baker, J.W., 2007: Quantitative classification of near-fault ground motions using wavelet analysis. *Bulletin of the Seismological Society of America*, 97, no. 5, 1486–1501.

APPENDIX A

MODAL PROPERTIES AND FREQUENCY RESPONSE FUNCTIONS OF EDI-OPTIMAL WHITE-NOISE BIS+TMDI

In explaining the beneficial effects of the grounded inerter to white noise excited TMD-equipped BIS it is instructive to examine the modal properties of EDI-optimal BIS+TMDI plotted in Figure A1 in the form of iso-curves on the μ-β plane. It is first observed that by increasing β for fixed μ the two damped pseudo-frequencies, Ω_1 and Ω_2, become better separated (i.e., Ω_1 shifts to lower frequencies and Ω_2 shifts to higher frequencies from ω_I natural frequency of the uncontrolled BIS simultaneously), while both pseudo-damping ratios increase. Collectively, these trends indicate that incorporating a grounded inerter with increasing inertance to the TMD yields an overall more efficient dynamic vibration absorber with increased bandwidth and damping capacity. Focusing on the second pseudo-damping ratio, η_2, it is seen that its value increases markedly with β and its iso-value curves are well-correlated with the $\xi_{T\,\mathrm{opt}}$ iso-value curves in Figure 6(b). Now, damping ratio η_2 is related with the second anti-resonant mode shape (i.e., modal ordinates have significant phase difference) and therefore leverages the dissipation capacity at the TMDI dashpot; clearly, the increased EDI values (and consequently the mitigation of BIS deflection and acceleration), as well as the reduced deflection and stroke of the secondary mass with β can be attributed to the large increase of η_2.

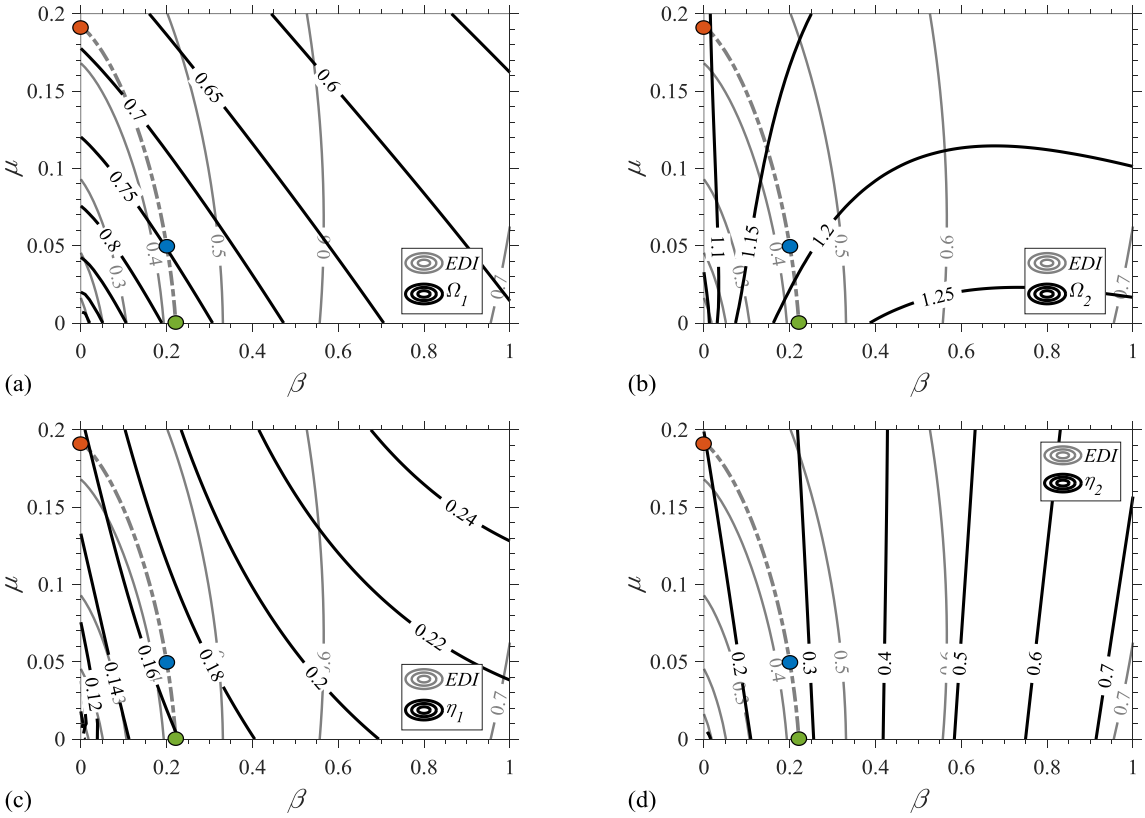

FIGURE A1 Optimal iso-value pseudo-frequencies (a),(b) and pseudo-damping coefficients (c), (d) on the μ-β TMDI inertial design plane of white noise excited BIS+TMDIs with ξ_I=0.15. EDI iso-value curves of Figure 5 are supersposed.

TABLE A1 Modal properties for the three particular EDI-optimal systems indicated in Figure 5.

Case	ν_{opt}	$\xi_{T\,opt}$	$s_i, \bar{s}_i$	Ω_i	η_i	$\psi_i, \bar{\psi}_i$
TMDI			-0.676 ± 2.389i	0.748	0.167	1.000 ± 0.000i 3.013 ± 0.767i
$\mu = 0.05$	0.887	0.268				
$\beta = 0.20$			-0.261 ± 1.545i	1.186	0.272	1.000 ± 0.000i -1.301 ± 0.517i
TID			-0.707 ± 2.454i	0.785	0.159	1.000 ± 0.000i 2.733 ± 0.598i
$\mu = 0$	0.957	0.267				
$\beta = 0.22$			-0.261 ± 1.623i	1.219	0.277	1.000 ± 0.000i -1.648 ± 0.553i
TMD			-0.453 ± 2.246i	0.690	0.155	1.000 ± 0.000i 5.599 ± 1.125i
$\mu = 0.19$	0.756	0.193				
$\beta = 0$			-0.224 ± 1.429i	1.094	0.198	1.000 ± 0.000i -0.926 ± 0.290i

Turning attention to the modal properties of the three particular TMD, TID, and TMDI secondary system designs with EDI=0.42, it is seen that while η_1 remains almost the same, η_2 increases by about 30% between the TMD and the TID and TMDI (see also Table A1). This significant increase of η_2 confirms that it is a valid explanatory factor for the improvement of inertial dampers performance, at least for suppressing BIS and secondary mass deflections. In this case, the beneficial effect of the inerter to mitigating secondary mass motion is further facilitated by the somewhat unexpected fact that both damped pseudo-frequencies, Ω_1 and Ω_2, increase with increasing β resulting in stiffer systems as one goes from the TMD to the TMDI to the TID. Now, the combination of faster dynamics (stiffer systems) with higher anti-resonant damping ratio η_2 justifies the decrease of secondary mass deflection and stroke (see Figures 7(c) and 7(d)) with increasing β for fixed EDI.

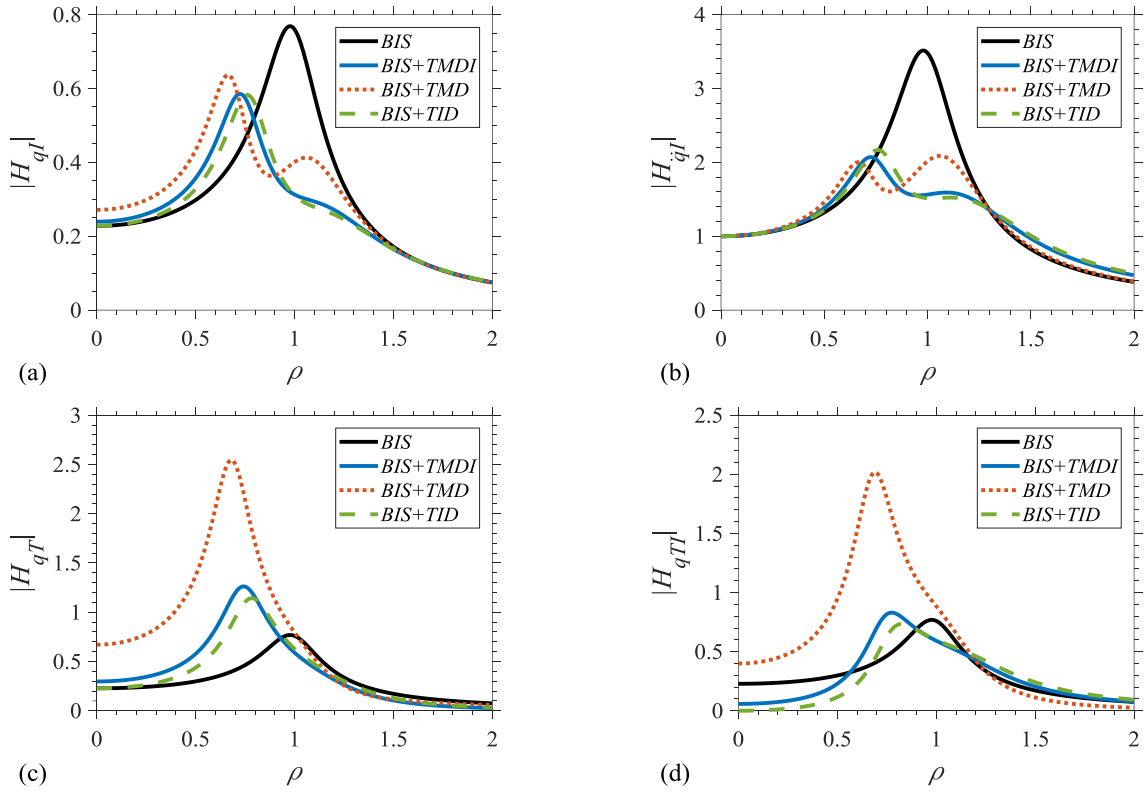

FIGURE A2 BIS displacement (a), BIS acceleration (b), secondary mass displacement (c) and secondary mass stroke (d) frequency response function for the three EDI-optimal white-noise excited systems indicated in Figure 5.

Moreover, Figure A2 provides frequency response functions (FRFs) in terms of relative to the ground BIS displacement, q_I, BIS acceleration, $\ddot{q}_I$, secondary mass displacement, q_T, and relative BIS to secondary mass displacement, q_{TI}, for the three EDI-optimal systems with EDI=0.42 discussed above. These plots confirm that the inclusion of a secondary mass to systems with appreciable inertance has little influence to the response of EDI-optimal BIS+TMDI systems, while the inclusion of a grounded inerter improves peak and RMS BIS displacement response while achieves significnat reductions to peak and RMS secondary mass kinematics.